
Doctoral Dissertations

Student Theses and Dissertations

Fall 2008

Friction stir channeling: an innovative technique for heat exchanger manufacturing

Nagarajan Balasubramanian

Follow this and additional works at: https://scholarsmine.mst.edu/doctoral_dissertations



Part of the [Mechanical Engineering Commons](#)

Department: Mechanical and Aerospace Engineering

Recommended Citation

Balasubramanian, Nagarajan, "Friction stir channeling: an innovative technique for heat exchanger manufacturing" (2008). *Doctoral Dissertations*. 1884.

https://scholarsmine.mst.edu/doctoral_dissertations/1884

This thesis is brought to you by Scholars' Mine, a service of the Missouri S&T Library and Learning Resources. This work is protected by U. S. Copyright Law. Unauthorized use including reproduction for redistribution requires the permission of the copyright holder. For more information, please contact scholarsmine@mst.edu.

FRICTION STIR CHANNELING: AN INNOVATIVE TECHNIQUE FOR HEAT
EXCHANGER MANUFACTURING

by

NAGARAJAN BALASUBRAMANIAN

A DISSERTATION

Presented to the Faculty of the Graduate School of the
MISSOURI UNIVERSITY OF SCIENCE & TECHNOLOGY

In Partial Fulfillment of the Requirements for the Degree

DOCTOR OF PHILOSOPHY

in

MECHANICAL ENGINEERING

2008

Approved by

K. Krishnamurthy, Co-advisor

Rajiv S. Mishra, Co-advisor

K. Chandrashekhara

Kakkattukuzhy M. Isaac

Robert G. Landers

PUBLICATION DISSERTATION OPTION

This dissertation has been prepared in the form of papers for publication. Each paper has been prepared in the style of the journal/proceeding to which it has been submitted. Four papers are selected to represent the doctorate work.

An “Introduction” section, pages 1-12, is included for presenting a brief background to this dissertation work. Section 2, pages 13-34, has been submitted as a paper to the Journal of Materials Processing Technology (Elsevier Science). Section 3, pages 35-54, has been prepared for submission to International Journal of Mechanical Sciences (Elsevier Science). Section 4 in pages 55-66 is prepared for submission to the Journal of Materials Processing Technology (Elsevier Science) and Paper IV, 67-81 has been prepared for publication in International Journal of Heat and Fluid Flow (Elsevier Science).

ABSTRACT

Friction stir processing (FSP) is an emerging processing technique based on the principles of friction stir welding (FSW), which is a relatively new solid-state metal joining process developed by The Welding Institute, UK. Some of the unique features of FSW such as the low amount of heat generated, extensive plastic deformation and controlled flow of material is being exploited to develop new material modification and manufacturing processes. Friction stir channeling (FSC) is one such adaptation of FSP that can produce continuous and stable internal channels for application in heat exchanging equipment. Friction stir channeling produces these channels if the defect formation and material flow are controlled during the FSW/P. Channel formation is also affected by other factors, including the process parameters, tool design, and material properties. A good understanding of the process forces, material flow, and metallurgy is therefore necessary to control and optimize the channel formation for use in heat exchangers.

The process forces acting on the tool during channeling were analyzed to study the channel formation mechanism and correlate the channel features to the process parameters and geometric features of the pin. A mechanistic model of the process specific energy was then developed and correlated to the channel size. Finally, the performance of the channels was experimentally determined by measuring the pressure drop across the channels and calculating the friction factor and heat transfer coefficient for different flow rates. These results will help develop the manufacturing process that will enable better control of the channel profile.

ACKNOWLEDGMENTS

I would like to acknowledge the help and support of many individuals in the preparation of this dissertation. First and foremost, I thank my advisors, Dr. Rajiv. S. Mishra and Dr. K. Krishnamurthy, for guiding my research over the past three-and-a-half years. They offered me the best possible facilities to conduct my research. Without their guidance, this work would not have been made possible.

I also thank Dr. K. Chandrashekhara, Dr. Kakkattukuzhy M. Isaac and Dr. Robert G. Landers, for guiding in my work and accepting to serve in my dissertation committee. I am grateful to the National Science Foundation (NSF) for supporting this research by way of their grant NSF-CMMI 0523022.

I would also like to thank members past and present of the Center for Friction Stir Processing at Missouri S&T for their support. Over the course of the past three and a half years, I had the opportunity to interact and gain knowledge from some of the brightest minds. They offered words of encouragement and support during some difficult phases I would always cherish the time I spent in their company.

Finally, my education would not have been possible without the support of my family. I dedicate this dissertation and degree to my parents K. N. Balasubramanian, and B. Lalitha and brother, B. Ganesan. I thank my teachers from past, and all my friends who shaped my thoughts and actions.

TABLE OF CONTENTS

	Page
PUBLICATION DISSERTATION OPTION.....	iii
ABSTRACT.....	iv
ACKNOWLEDGMENTS	v
LIST OF ILLUSTRATIONS.....	viii
LIST OF TABLES.....	x
1. INTRODUCTION	1
1.1. BACKGROUND	1
1.2. LITERATURE SURVEY.....	5
1.2.1. Heat Exchanger Performance.....	5
1.2.2. Modeling of Friction Stir Channeling	8
1.3. SCOPE OF THE DISSERTATION	12
1.3.1. Characterization of the Channels	12
1.3.2. Process Forces	12
1.3.3. Mechanistic Modeling.....	12
1.3.4. Performance of the Channels	12
2.FRICTION STIR CHANNELING: CHARACTERIZATION OF THE CHANNELS	13
2.1. INTRODUCTION	14
2.2. EXPERIMENTAL PROCEDURE.....	17
2.3. RESULTS AND DISCUSSION.....	18
2.3.1. Channel formation.....	18
2.3.2. Channel shape.....	19
2.3.3. Channel size	22
2.3.4. Surface roughness.....	25
2.3.5. Channels along curves.....	27
2.3.6. Mechanical properties	30
2.4. FINISHING PROCESS	32
2.5. CONCLUSION.....	32
2.6. ACKNOWLEDGMENT	32
2.7. REFERENCES	32

3. PROCESS FORCES DURING FRICTION STIR CHANNELING IN AN ALUMINUM ALLOY	35
3.1. INTRODUCTION	35
3.2. EXPERIMENTAL PROCEDURE	38
3.3. RESULTS AND DISCUSSION.....	40
3.3.1. Macrostructure.....	40
3.3.2. Polar Plots.....	42
3.3.3. Force Signature.....	48
3.4. Conclusion	52
3.5. Acknowledgement	52
3.6. REFERENCES	52
4. DEVELOPMENT OF A MECHANISTIC MODEL FOR FRICTION STIR CHANNELING	55
4.1. INTRODUCTION	55
4.2. EXPERIMENTAL SET-UP	57
4.3. RESULTS AND DISCUSSION.....	58
4.3.1. Specific energy	58
4.3.2. Surface temperature profile	60
4.3.3. Channel area	63
4.4. CONCLUSIONS	65
4.5. ACKNOWLEDGEMENT	65
4.6. REFERENCES	65
5. STUDY OF THE PRESSURE DROP AND HEAT TRANSFER THROUGH A FRICTION STIRRED CHANNEL	67
5.1. INTRODUCTION	67
5.2. EXPERIMENTAL SET-UP	70
5.3. RESULTS AND DISCUSSION.....	72
5.4. CONCLUSION.....	79
5.5. ACKNOWLEDGMENTS	79
5.6. REFERENCES	80
6. CONCLUSIONS AND SCOPE OF FUTURE WORK.....	82
7. BIBLIOGRAPHY	83
VITA	88

LIST OF ILLUSTRATIONS

Figure	Page
1.1. Schematic Representation of Friction Stir Welding.	2
1.2 Model showing the relationship between process variables and physical effects.	4
2.1 Cross-sectional image of a channel showing the different process regions: (A+B) channel nugget, (C) parent material, (D) channel, and (E) material from the channel nugget deposited on the surface.	19
2.2 Cross section showing the channel shapes at different processing parameters: (a) 1100 rpm, 2.11 mm/sec, and (b) 1100 rpm, 2.96 mm/sec.	20
2.3 Force plots for (a) 1100 rpm and 2.11 mm/sec, and (b) 1100 rpm and 2.96 mm/sec.	21
2.4 Variation of the channel area for different process pitches for the three tools at a depth of 3.0 mm.	23
2.5 Variation of area of the channel with traverse speed and rotational speed at depths of (a) 2.8 mm and (b) 3 mm for the tool 1. The numbers on contour lines represent the area of the channels in mm ²	24
2.6 Variation of the channel hydraulic diameter for different process pitches for the three tools at a depth of 3.0 mm.	25
2.7 Longitudinal cross section of the channel showing the roughness on the roof of the channels. (a) 1200 rpm, 2.11 mm/sec, (b) 800 rpm, 1.27 mm/sec and (c) 800 rpm, 0.42 mm/sec.	26
2.8 Cross sections of the channel at different locations along the curve in a serpentine profile with the advancing side on (a) the outer curve, and (b) the inner curve. ω represents the tool rotation direction and v represents the traverse direction.	28
2.9 Variation of the channel's cross-sectional area and the area of material deposited on top of the parent material along the curve in the serpentine profile.	29
2.10 Strength of material on the roof of the channel along the longitudinal direction, (b) elongation of material on the roof of the channel along the longitudinal direction.	30
2.11 Microhardness profile across the channel nugget processed by tool 3 for different heat indices.	31
3.1 Cross-sectional image of a channel.	37
3.2 Plot showing the variation of the cross-sectional area of the channels for the three tools, as a function of the heat index.	42
3.3 A Schematic representation of friction stir channeling and co-ordinate system of the FSC forces measured using the high-frequency data acquisition.	43
3.4 Polar plots of the resultant forces (units - N) during FSC of Al6061-T6 using FSC11.	45

3.5 Polar plots of the resultant forces (units - N) during FSC of Al6061-T6 using FSC12.....	46
3.6 Polar plots of the resultant forces (units - N) during FSC of Al6061-T6 using FSC13.....	47
3.7 Force plots for 1200 rpm and 2.11 mm/sec using FSC12 with an inset of the channel. Shaded region shows the force profile for one complete rotation of the tool.....	48
3.8 Force plots for 1200 rpm and 2.96 mm/sec using FSC12 with an inset of the channel. Shaded region shows the force profile for one complete rotation of the tool.....	49
3.9 SEM of the material on the roof of the channel processed at 1100 rpm and 2.96 mm/sec using FSC12.....	51
3.10 Force plots for 1100 rpm and 2.96 mm/sec using FSC12 with an inset of the channel. The SEM of the channel roof is overlaid. Shaded region shows the force profile for one complete rotation of the tool.	51
4.1 Variation of the peak temperatures against pseudo heat index along (a) advancing side, and (b) retreating side.	61
4.2 Variation of the peak temperatures against specific energy along (a) advancing side, and (b) retreating side.	62
4.3 Variation of the channel area as a function of (a) pseudo heat index, and (b) specific energy.....	64
5.1 A schematic of the experimental setup.....	72
5.2 Cross-section of the channels depicting the variation of channel shapes with processing parameters. (a) 1100 rpm, 2.96 mm/sec and (b) 1200 rpm, 2.11 mm/sec.....	72
5.3 Longitudinal cross-section of the channel showing the roughness on the roof of the channels (1200 rpm, 2.11 mm/sec).....	73
5.4 Measured pressure drop for channels with different hydraulic diameters.....	74
5.5 Plot of the calculated heat transfer coefficient for the different channels at different flow rates.	75
5.6 Measured heat transfer coefficient of the channels.....	76
5.7 Measured pressure drop across the channels along curves.....	77
5.8 Simulated pressure drop along linear channels with different hydraulic diameters. ...	78
5.9 Simulated pressure drop across channels along curves and with different hydraulic diameters.....	79

LIST OF TABLES

Table	Page
1.1 Channel Classification [17].....	6
2.1 Channel classification (Kandlikar and Grande, 2004).....	17
3.1 Dimensions of the friction stir channeling tools.....	39
3.2 Processing parameters.....	40
3.3 Channel features for Al6061-T6 processed using FSC. The numbers indicate the area of the channel in mm ²	41
4.1 Processing parameters.....	57
4.2 List of process parameters with the measured and modelled torque, spindle power and specific energy.	60
5.1 Channel Classification [14].....	70
5.2 Range of experimental parameters investigated. All tests were conducted with the water as the test fluid.....	71

1. INTRODUCTION

1.1. BACKGROUND

Friction stir welding (FSW) is a solid state metal joining technique invented in 1991 and patented by The Welding Institute, United Kingdom [1]. This environmentally friendly and energy efficient technique can be used to join high strength aerospace aluminum alloys and other metallic alloys that are difficult to join using conventional metal joining techniques. Another advantage of this technique is it does not use filler material, leading to significant weight reduction.

Figure 1.1 is a schematic of the FSW process. The process works by traversing a non-consumable, rotating tool under the action of a vertical load along the joint of workpieces. The rotating tool penetrates into the work-piece surface making surface to surface contact, thus generating frictional heat at the tool-work material interface, thereby reducing the material flow stress. The tool geometry and process parameters determine the direction and pattern of material flow and have been described in detail by London et al. [2].

The tool used in FSW has two distinct parts - the shoulder and the pin, and is designed to serve three functions: a) generate frictional or deformational heat that softens the work material ahead of the pin; b) control the material flow to produce a defect free joint; and c) contain the hot material under the shoulder. The rotation of the shoulder and pin generates heat because of friction and severe plastic deformation of workpiece. This heating softens the material around the pin and the combination of tool rotation and traverse movement displaces the material from the front to the back of the pin. Besides the pin, the shoulder also applies a forging force on the material behind the pin, effectively filling the cavity formed by the forward motion of pin. The shoulder is designed to generate sufficient frictional and deformational heat in thin sheets, while the pin produces the bulk of the heat in thick workpieces. Features are incorporated on the shoulder and pin surfaces to further aid these functionalities.

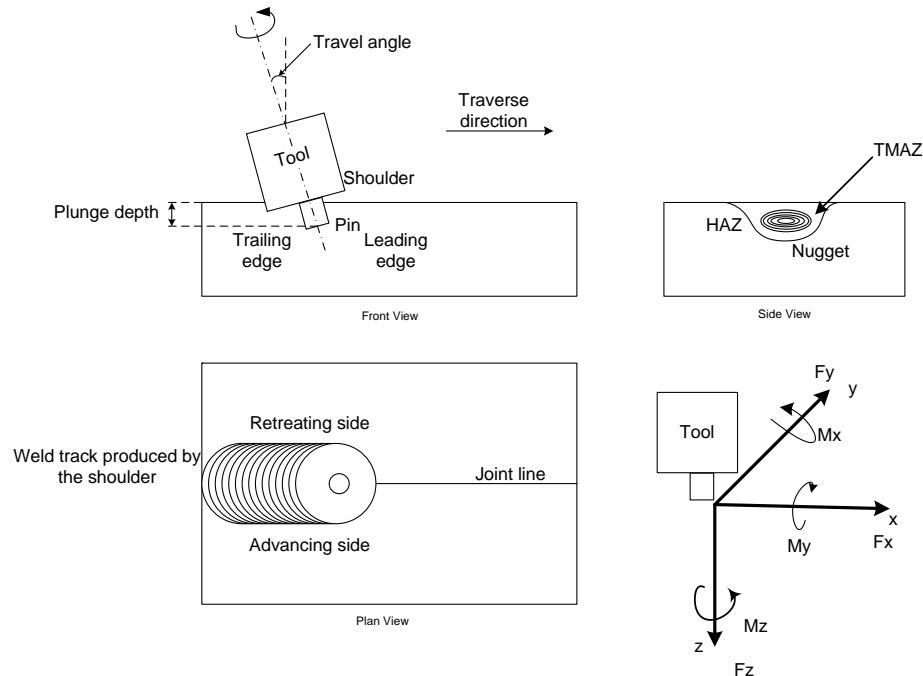


Figure 1.1. Schematic Representation of Friction Stir Welding.

A strong and defect-free friction stir weld with good surface finish can thus be produced by choosing a proper tool profile and optimal processing parameters [3]. The choice of tool profile affects the volume of the processed region, the flow pattern of the material around pin and the occurrence of defects. Apart from the tool variables, five other processing parameters controlled in FSW are: a) tool rotational rate; b) tool travel speed; c) plunge depth; d) travel angle; and e) work angle. These parameters determine the strength and finish of the weld joints. The tool rotation and travel speed control the amount of plastic deformation and subsequent frictional and deformational heat generated. These two parameters, along with plunge depth, affect the axial force imparted on workpiece which significantly affects the weld quality [4]. The tool is given a travel angle during traverse to help improve the consolidation of material along the pin's wake.

Friction stir processing (FSP) is an adaptation of FSW utilizing some of its unique features like fine grain size in the stirred region, extensive plastic flow of material, low amount of heat generated, absence of flaws and pores, and mechanical mixing of the surface and subsurface layers to develop new processes [5]. Friction stir channeling

(FSC) is a modification of FSP that gainfully utilizes the process of wormhole formation during FSW to fabricate continuous and stable channels. The characteristics of these channels can be altered by controlling the process parameters. This process is capable of generating a continuous channel in monolithic plates along the travel path of the tool. Arbegast [6] has studied the formation of these wormholes and other defects in FSW and analyzed the causes behind their formation. Mishra [7] showed that this process can be used as a technique to manufacture continuous channels for use in heat exchanging applications.

A major area of research in FSW/P is process modeling. A predictive model of the process can be used to develop new tool designs that will enable optimal process outputs for different work materials and process parameter combinations. Various process modeling techniques based on analytical, numerical and mechanistic theories have been developed and presented in the literature. Numerical models are more commonly used than analytical models due to their ease of use. Moreover, numerical models are capable of capturing much of the complexities involved in FSW/P processes, such as material flow behavior, thermal boundary condition in relation to tool and fixture geometry, and material properties. However, these models need powerful computational resources and time. When using any of these techniques, it is necessary for users to keep the goals of the model in perspective and adopt the appropriate level of complexity. Colligan [8] developed a conceptual model that relates the process variables to the metallurgical, mechanical and heat transfer aspects of the process. The model describes the interaction between the physical effects and workpiece flow stress, welding torque, heat generation, and temperature during FSW process. Shercliff et al. [9] has also developed a model highlighting the key physical interactions in FSW linking process input parameters to the output needed by the designers. In posing a viewpoint questionnaire, Mishra [10] has summarized the various aspects of the friction stir process. The viewpoint paper address some of the critical questions facing the friction stir researchers and illustrates the inter-relationship between the process; the thermal, deformational, frictional, and material flow aspects; and the resultant microstructure, flow pattern, and temperature due to deformational heating. Figure 1.2 shows the

relationship between process variables and physical effects combining both Colligan and Mishra's models.

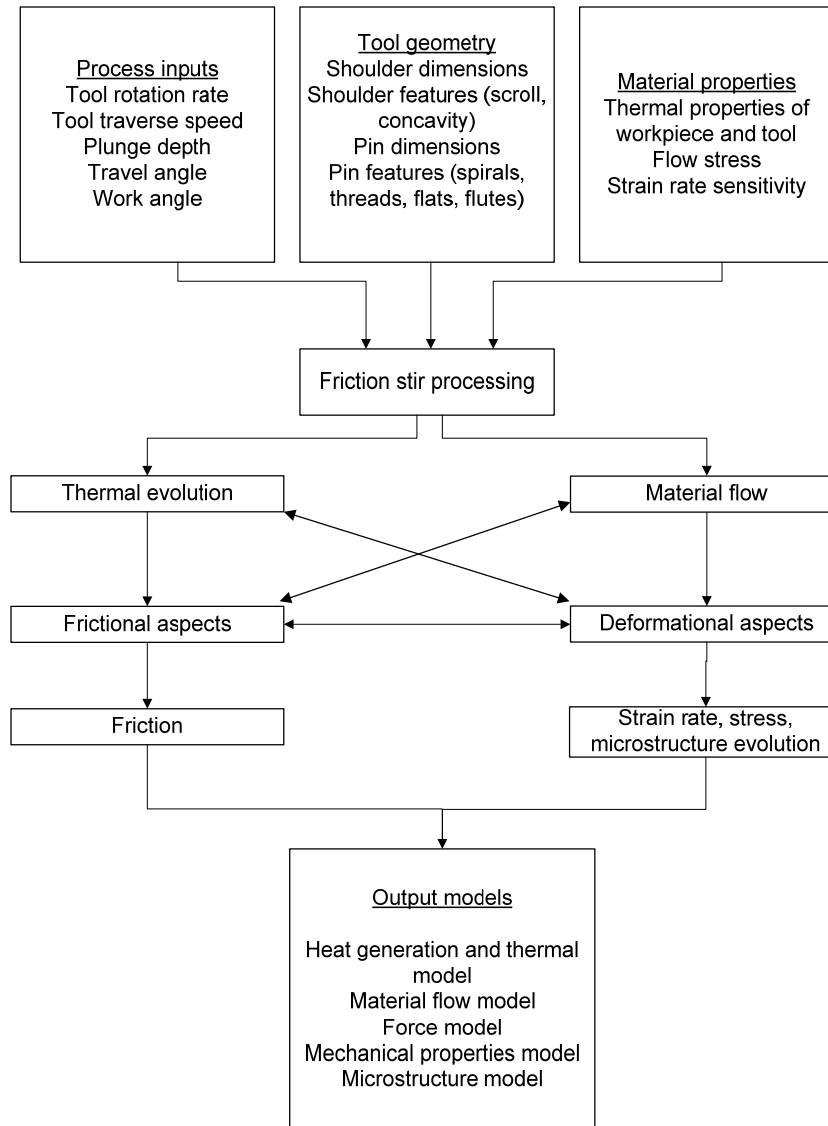


Figure 1.2 Model showing the relationship between process variables and physical effects.

This dissertation investigates the different features of the channels generated using FSC process. There were four main objectives of this study: (a) to understand the channel characteristics and their relationship with the process parameters and different

tool features; (b) to understand the channel formation by studying variation of the process forces; (c) to develop a mechanistic model of the process specific energy to correlate against the channel size; and (d) measure the channel's performance under different flow conditions by experimentally determining the friction factor and heat transfer coefficient for different channel profiles. The overarching goal of this study was to develop a manufacturing process that will enable a better control of the channel profile.

1.2. LITERATURE SURVEY

1.2.1. Heat Exchanger Performance. Heat exchangers are devices used to transfer thermal energy between two or more fluids or between a solid surface and a fluid at different temperatures [11]. They are built for efficient heat transfer from one medium to another, where the media are usually separated by a solid wall to prevent any mixing [12]. Heat exchangers are widely used in refrigeration, air conditioning, power plants, chemical plants, petrochemical plants, refineries, and automobiles. An example of a heat exchanger is an automobile radiator, in which the engine cooling fluid transfers heat from the engine surface to air flowing through the radiator fins. Heat exchangers are usually classified on the basis of their transfer process as either direct contact or indirect contact, number of process fluids used, construction and flow arrangements, or heat transfer mechanisms. Another means of classifying heat exchangers is by their surface compactness. Compact heat exchangers (CHE) thus evolved with the need for reducing the physical size and weight for an overall improved performance. These heat exchangers have fluid flow passages that vary from a few millimeters to microns in diameter. Compact heat exchangers with mini-channels have been applied in fuel cells, micro-electronics, aerospace components, micro fabricated fluidic systems, and other applications that require small volume and light weight [13, 14]. The surface area-to-volume ratio (A/V) is an indicator of the heat exchanger's compactness, and is usually used in studies on this topic. The surface area density for compact heat exchanges is greater than $700 \text{ m}^2/\text{m}^3$ [15].

As mentioned earlier, compact heat exchangers have channels of different sizes and are usually classified on the basis of their channel dimensions. The important characteristic dimensions of a channel are the distance between the heat sink and heat

source and the hydraulic diameter, D_h . Hydraulic diameter is a term commonly used for measuring flow in noncircular tubes and channels and is defined as the ratio of four times the area of the cross-section to the wetted perimeter of the channel. On the basis of channel dimensions, further classifications of compact heat exchangers have been proposed by various researchers. Mehendale [16] classified CHEs on the basis of their hydraulic diameters as

- micro-channels - 1 μm to 100 μm
- meso-channels - 100 μm to 1 mm, and
- conventional passages - >6 mm.

Kandlikar et al. [17] proposed a classification scheme that replaces the channel hydraulic diameter with the minimum channel dimension (D), as shown in Table 1.1. Kawahara et al. [18] studied the variation of void fractions in two-phase flows for varying hydraulic diameters and concluded that the transition boundary between the micro- and mini-channels lies between $D_h = 100 \mu\text{m}$ and $D_h = 251 \mu\text{m}$.

Table 1.1 Channel Classification [17]

Conventional channels	$D > 3 \text{ mm}$
Mini-channels	$3 \text{ mm} \geq D > 200 \mu\text{m}$
Micro-channels	$200 \mu\text{m} \geq D > 10 \mu\text{m}$
Transitional channels	$10 \mu\text{m} \geq D > 0.1 \mu\text{m}$
Transitional micro-channels	$10 \mu\text{m} \geq D > 1 \mu\text{m}$
Transitional nano-channels	$1 \mu\text{m} \geq D > 0.1 \mu\text{m}$
Molecular nano-channels	$0.1 \mu\text{m} > D$

Wadekar [19] has discussed the current manufacturing techniques used for different commercial heat exchangers. Conventional shell and tube heat exchangers are made from 8 mm to 60 mm diameter tubes that are joined using welding and other metal joining processes. The plate heat exchangers have a hydraulic diameter of 5 to 6 mm and are also joined using welding, brazing, and other conventional techniques. Tube-fin and

Plate-fin heat exchangers (for example, car radiators) have a typical diameter of 2 to 3 mm, and are fabricated using brazing. Printed circuit heat exchangers (PCHE) have channels with hydraulic diameters of 1 to 2 mm. Diffusion bonding and brazing techniques are used for PCHEs. Compact heat exchangers with micro- and meso-scale channels are generally manufactured using techniques like chemical etching, micro-fabrication, precision machining, and selective laser melting [20, 21]. These compact heat exchangers are designed to maximize the surface area density of channels for any application. Also, the channels can traverse different geometric profiles, such as linear or serpentine with curvy bends or right angle bends, to effectively utilize the available surface area.

For heat exchangers with micro- and mini-channels, the principles of heat exchanger design have been applied to micro-scale devices, resulting in basic designs comparable to those of macro-scale devices, such as cross-flow or counter-flow heat exchangers, but with much smaller characteristic dimensions [22]. To prove that FSC is a viable alternative to existing manufacturing techniques for developing compact heat exchangers, the pressure drop along the length of channels and the heat transfer coefficient of the heat exchanger assembly should compare favorably with existing heat exchangers. The channels generated using FSC do not usually conform to shapes such as circles, quadrilaterals or ellipses. Also, the inner surfaces of these channels have surface roughness features along their length. The non-conformal shape of the channels and the presence of roughness features on the channel interior make the channel's performance too complex for a heat exchanger application.

The literature abounds with both experimental and numerical analysis on the pressure drop and heat transfer performance of many heat exchangers. Adams et al. [23] conducted single-phase flow studies in micro-channels using water as the working fluid. Peng et al. [24] investigated the water flow in rectangular micro-channels with hydraulic diameters ranging from 0.133 to 0.367 mm. In laminar flow, heat transfer depends on the aspect ratio of the channels and the ratio of hydraulic diameter to the center-to-center distance of the micro-channels. The effects of surface roughness on pressure drop in circular tubes and rectangular channels have been studied extensively. In the nineteenth century, Darcy [25] conducted pressure drop experiments on pipes of different materials

and roughness, introducing the concept of relative roughness, and concluded that fluid flow depends on the pipe roughness, diameter, and slope. Fanning [26] proposed a correlation for the pressure drop as a function of surface roughness. Nikuradse [27] established the sand-grain roughness as a critical parameter affecting friction factor during laminar and turbulent flows. Kandlikar et al. [28] has further characterized the surface roughness effects on pressure drop in single-phase flow in mini-channels.

Channels made using FSC have a hydraulic diameter ranging from 0.2 to 2 mm and, therefore, fall in the mini-channels category according to Kandlikar's classification [17]. Wang et al. [29] studied the performance of mini-channel heat exchangers using experimental techniques. The heat exchangers in their study had a high surface area density of $1500 \text{ m}^2/\text{m}^3$ and a heat transfer coefficient of around $7 \text{ MW}/\text{m}^3 \text{ }^\circ\text{C}$. Westphalen et al. [30] studied the benefits of using aluminum alloys for mini-channel heat exchangers. They identified the improved heat exchanger corrosion resistance and the ease of leak repair with epoxy in these heat exchangers. These researchers also recognized the need for having multiple coils of mini-channels to obtain performance equivalent to conventional heat exchangers. Kandlikar [31] provided a roadmap for mini-channel implementation in residential, commercial, and industrial refrigeration and air-conditioning systems.

1.2.2. Modeling of Friction Stir Channeling. Material flow around the friction stir tool during FSP is closely related to many of the key process issues. The coefficient of friction at tool-workpiece interface, strain and strain rate of the deformed work material are all closely interconnected to the flow condition. Since FSP is a coupled thermomechanical process, the thermal history is also intertwined with the flow pattern. The channel formation in FSC is caused by the presence of discontinuities in the material flow field, and knowledge of the material flow pattern is therefore a critical component in understanding the effect of different process parameters and tool profiles for this process. Analysis of the development of forces and moments for different inputs further aids this study.

Many flow visualization studies [32] and numerical analyses [33, 34] have been done to comprehend the material flow behavior. Frigaard et al. [35] developed a finite difference method based model for energy generated using the interfacial pressure and

tool radius without considering the effect of pin. Most of the initial studies in literature involved quantitative analysis of peak temperature and were based on the heat conduction theory. The heat generated during FSW/P is generally assumed to be the combination of two different mechanisms: (i) friction at the tool-workpiece interface and (ii) the plastic deformation of the workpiece. Heat generated by these two processes is dissipated into the material around pin by conduction, thus softening the workpiece. Knowledge of thermal history thus constitutes a critical component in the understanding of mechanical property evolution in different regions of the nugget. Khandkar et al. [36] developed a model that correlated the heat input with measured torque by assuming uniform shear stress at the tool-workpiece interface. The heat input is defined by the relation

$$\dot{Q}_{interface} = \dot{Q}_{tot} \times \frac{\text{Torque generated by the interfacial area}}{\text{Total torque}} \quad (1)$$

where, $Q_{interface}$ represents the heat input at the interface and Q_{tot} is the total heat input. They concluded that the heat from the tool-workpiece interface flows along a vertical path into the backing plate. Seidel et al [37] further developed this model, accounting for the conical shouldered tools and by classifying the surface based on vertical and horizontal orientations.

Another quantitative study on temperature field and peak temperature conducted by Schmidt et al. [38] was also based on heat conduction theory, but has ignored the plastic flow of material near the tool. This theory characterizes the material flow and heat generation around pin according to the contact conditions at tool-workpiece interface. Three frictional conditions are described in this model: sliding, sticking, and partial sliding/sticking. According to the model, the shoulder-material interface is the major source of heat generation (86 %) compared to the pin sides-workpiece (11 %) or pin tip-workpiece interface (3 %). This model therefore infers that heat generation is a function of tool design. Heurtier et al. [39] tried to predict heat generation based on plastic strain, shoulder friction, and pin friction.

Arbegas [40] studied the effect of process parameters on temperature. For a given tool geometry and plunge depth, the maximum surface temperature was a function of the

traverse speed. On the basis of his work, the relationship between the maximum welding temperature and the process parameters is given by

$$\frac{T}{T_m} = K \left[\frac{\omega^2}{v \times 10^4} \right]^a \quad (2)$$

where ω is the tool rotation rate, v is the tool traverse speed, T is the maximum welding temperature, T_m is the melting point of the alloy and a and K are constants. ω^2/v is referred to as the pseudo heat index. The value of a ranges from 0.04 to 0.06, and the constant K varies between 0.65 and 0.75. Generally the maximum temperature observed during FSW of various aluminum alloys is between $0.6 T_m$ and $0.9 T_m$. This model fits temperature values well, but is limited to specific tool sizes. It cannot predict temperature variation with changes in tool size, even for the same tool design.

Roy et al. [41] developed a dimensionless correlation based on Buckingham's π – theorem to estimate the peak temperature during FSW. They proposed a new relationship between the dimensionless heat input and the dimensionless peak temperature that also accounts for the change in tool size. It is given

$$Q^* = f \sigma_8 A \omega C_p / k U^2 \quad (3)$$

where Q^* is the dimensionless heat input, f is defined as ratio of heat generated at the tool shoulder-workpiece interface, σ_8 is the yield stress of work material at $0.8 T_s$ (solidus temperature), A the area of tool shoulder, k/C_p is the thermal property of the alloy, ω is the angular velocity, and U is the translational velocity.

McClure et al. [42] presented a thermal field generation model based on Rosenthal's moving point source equation [43] and compared it to experimental results. Kalya et al. [44] developed a model to calculate specific energy as a function of the process parameters, on the basis of which they studied the surface temperature of the work material lateral to the motion of the tool. Long et al. [45] studied the effects of varying material properties and process parameters on the trends in x axis forces and

potential weld defect formation (via a material flow patterns) by fluid dynamics simulation.

During friction stir processing, forces, moments and torque acting on the tool spindle vary with process parameters. The signature created by variation of these process variables offers insight into the working mechanism of FSW/P. Using force patterns to analyze the material flow behavior is a relatively new development in FSW/P. Yan et al [46] studied the relationship between periodicity of process parameters and that of micro- and meso-structural banding in FSW. They measured and analyzed the oscillation of FSW parameters during baseline experiments without welding and during a series of FSW of AA2524 and AA2024 aluminum alloys and characterized the banded structures in all the welds. The measured band spacing was correlated with the oscillation period of process forces F_x and F_z exerted on and by the welding tool. Blignaut et al. [47] discussed the development of a multi-axial transducer capable of capturing the process force foot print that can be used to measure the energy input to the welding. Hattingh et al. [48] analyzed the force foot prints to systematically study the influence of tool geometry factors on FSW process parameters and weld tensile strength, thereby optimizing the tool design to produce welds with 97 % of the parent plate tensile strength in Al 5083-H321 alloy. Arbegast [49] experimentally demonstrated the change in process forces due to clamping locations, welding direction, crossing over pre-existing FSW and change in the process parameters (rotation rate and traverse speed). Hattingh et al. [50] have also studied the relationship between tool profile, rotational rate, traverse speed, and microstructure using force foot print plots. They developed polar plots which show the force vector experienced by the tool during each revolution.

Analyzing the development of forces and moments for different processing parameters also helps in understanding the channel development. This dissertation describes a study of the force patterns during processing in an effort to explain material flow behavior and heat generation. A model that correlates the channel characteristics with the process parameters for different tool profiles has been developed from basic principles.

1.3. SCOPE OF THE DISSERTATION

The focus of this study is on four areas related to FSC: (1) characterization of FSC, (2) understanding the channel formation, (3) mechanistic modeling of FSC, and (4) performance evaluation of the FSC channels. Understanding each of these aspects is necessary to predict FSC's viability as a heat exchanger manufacturing process. This dissertation is organized into papers on channel characterization, study of process forces, channel performance, and mechanistic modeling of the process.

1.3.1. Characterization of the Channels. The channels created by the FSC processes were analyzed for the different features such as shape, size, hydraulic diameter, and interior roughness profiles. An empirical model relating the process parameters to the channel features was developed from experimental data and studied. The continuity and the stability of the channels along linear and curvilinear profiles were verified for different input parameters.

1.3.2. Process Forces. In this paper, the correlation of forces measured during the FSC process to the channel geometries is described. Force patterns were recorded using a high frequency data acquisition system connected to the head of a friction stir spindle. Polar plots of the resultant forces acting on the tool spindle were studied to understand the force vector acting on the tool. Variation in force patterns for different process parameters and different tool profiles were examined. The process force was used as a tool to help understand the material flow behavior in the channel formation process.

1.3.3. Mechanistic Modeling. A mechanistic model for the process specific energy as a function of the processing parameters during FSC was developed and investigated. The thermal cycle acting on the surface of the workpiece was measured using an IR camera and the peak temperatures were studied as a function of the specific energy. The channel area is plotted against the process specific energy and analyzed. A relationship between the processing conditions and the channel area was defined.

1.3.4. Performance of the Channels. Channel performance was studied to calculate the heat transfer coefficient of a test set-up. Pressure and thermal losses along the length of linear and serpentine channels are described in this paper. The effect of roughness on the pressure losses was analyzed for different flow rates. The experimental results were compared to solutions from the commercial CFD package, FLUENT.

2. FRICTION STIR CHANNELING: CHARACTERIZATION OF THE CHANNELS

N. Balasubramanian¹, R. S. Mishra^{2,‡}, K. Krishnamurthy¹

¹ Department of Mechanical and Aerospace Engineering, Missouri University of Science and Technology, Rolla, MO 65409, USA

² Center for Friction Stir Processing, Department of Materials Science and Engineering, Missouri University of Science and Technology, Rolla, MO 65409, USA

ABSTRACT

Commercially available compact heat exchangers are currently fabricated in several steps by joining multiple tubes, or by independently fabricating and joining fluid channels. Friction stir channeling (FSC) is a simple and innovative technique of manufacturing heat exchangers in a single step by creating continuous, integral channels in a monolithic plate in a single pass. FSC relies on the frictional heat generated between the tool material and the metal workpiece to soften and deform the material to facilitate the creation of a continuous channel. The channel shape, size, and integrity depend on the processing parameters and the tool design. In this paper the structural characteristics and the relationship between the channel features and the processing parameters are discussed. FSC is being developed as a technique for manufacturing heat exchangers. The channel is characterized by roughness features on the inside, which can be analyzed using optical microscopy techniques.

Keywords: friction stir processing; friction stir welding; heat exchangers; minichannels

[‡] Corresponding author. Tel.: +1-573-341-6361; e-mail: rsmishra@mst.edu

2.1. INTRODUCTION

Friction stir welding (FSW) and friction stir processing (FSP) are emerging as very effective solid state joining/processing techniques. FSW was invented at The Welding Institute (TWI) of UK in 1991 as a solid-state joining technique, and it was initially applied to aluminum alloys (Thomas et al., 1991). In this process, a non-consumable rotating tool with a pin and shoulder is inserted into the abutting edges of the sheets to be joined and traversed along the line of joint. Frictional and deformational heat is generated due to tool - work material interaction. The combination of the tool rotation and tool traverse moves the material from the front of the pin to the back of the pin. During this process, the material undergoes intense plastic deformation at an elevated temperature and results in a fine-grained microstructure in the stirred region (called a “nugget”) (Reynolds, 2007). FSP is an adaptation of FSW and is used as a generic tool for microstructural modification of materials based on the principles of FSW. Some of the unique features of FSW such as the low amount of heat generated, extensive plastic deformation and controlled flow of material is being used to develop new material modification and manufacturing processes (Mishra and Ma, 2005).

During FSW, a defect referred to as a “wormhole” is generated if the processing parameters and tool shoulder contact are not proper. FSC is based on converting this defect formation process into a manufacturing technique for heat exchanger applications. Mishra (2005) has shown that a continuous hole in a single plate can be achieved by selecting the right processing conditions and reversing the material flow. The main aspects of FSC are as follows:

- a) the profiled tool is rotated such that the material flow is upwards towards the tool shoulder;
- b) an initial clearance is provided between the shoulder and the workpiece, where the material from the base of the pin is deposited; and
- c) this distance between the tool shoulder and the workpiece can be adjusted to control the shape, size, and integrity of the channel.

The presence of the gap between the shoulder and the workpiece is a major difference between the FSC and the normal FSW or FSP practices where the back of the shoulder touches the workpiece to generate the forging action required to produce defect-

free welding or processing. During channeling, an upward force is generated by rotating a right-hand threaded tool clockwise (or a left-hand threaded tool counter-clockwise). A channel is formed because of the separation of the plasticized material around the pin from the plasticized material at the base of the pin. This separated material is moved upwards by the rotation of the pin and the orientation of the threads, and it is deposited on the top of the nugget underneath the shoulder surface. The shape and size of the channel can be controlled by varying the following parameters: The clearance between the shoulder and the work material; the tool rotation speed; the tool traverse rate and the tool design.

The generation of a continuous channel by FSC has the potential to open a wide range of applications in heat exchanger industry. Heat exchangers are devices that are used to transfer thermal energy between two or more fluids, or between a solid surface and a fluid, at different temperatures and in thermal contact (Shah and Sekulic, 2003). Typical applications of heat exchangers involve heating or cooling of a fluid stream and evaporation or condensation of fluid streams, with an objective to reject or recover heat. Heat exchangers are usually classified on the basis of the transfer process, as either direct contact type or indirect contact type. The heat exchangers are also classified on the basis of the number of process fluids, or on the basis of the construction or flow arrangements or the heat transfer mechanisms. Another basis for classification of the heat exchangers is on the basis of surface compactness. The main objectives of compact heat exchangers are to maximize the efficiency of a heat exchanger and also to reduce the size of the heat exchanger for a given duty. Compact heat exchangers are generally used in industry, especially in gas-to-gas or liquid-to-gas heat exchangers. For example, vehicular heat exchangers, condensers and evaporators in air-condition and refrigeration industry, aircraft oil-coolers, automotive radiators, and intercoolers or compressors.

Compact heat exchangers are generally used in gas flow applications. These heat exchangers have a surface area density higher than $700 \text{ m}^2/\text{m}^3$; i.e., they have a higher heat transfer surface area per unit volume. The principles of heat exchanger design have been applied to micro-scale devices, resulting in basic designs comparable to those known from macro-scale devices, such as cross-flow or counter-flow heat exchangers, but providing much smaller characteristic dimensions (Bradner et al., 2006). Wadekar

(2005) has examined industrial heat exchangers where mini- and microscale heat transfer are of significance. The most important of these characteristic dimensions are the distance between heat sink and heat source, and the hydraulic diameter D_h . The hydraulic diameter is a term commonly used when handling flow in noncircular tubes and channels and is defined as the ratio of four times the area of the cross-section to the wetted perimeter of the channel. On the basis of the hydraulic diameter, compact heat exchangers have been classified into micro-heat exchangers ($D_h = 1 - 100$ microns), meso-heat exchangers ($D_h = 0.0001 - 1$ mm), compact heat exchangers ($D_h = 1 - 6$ mm) and conventional heat exchangers ($D_h > 6$ mm) (Mehendale et al., 2000). A different system of classification on the basis of the minimum channel dimension (D) has been proposed by Kandlikar and Grande (2004) as shown in Table 2.1. The channels obtained using FSC have a D of 0.2 mm to 2 mm and therefore fall in the minichannels category on the basis of Kandlikar's classification. Also the friction stir channels have irregular shapes and fluid flow through irregular geometries has been dealt extensively in the literature. Wu and Cheng (2003) have studied the flow characteristics inside trapezoidal microchannels with different aspect ratios. Li et al. (2006) have performed numerical simulations of the flow and heat transfer of fluids inside microchannels with non-circular cross sections (trapezoidal and triangular). Hrnjak and Tu (2007) have summarized the list of experimental studies that have been done in regular and irregular shaped microchannels and studied the pressure drop inside rectangular microchannels at different flow rates and for different test fluids.

Presently, compact heat exchangers are manufactured using metal removal processes like micromachining and are later assembled and joined using metal joining techniques. Tsopanos et al. (2005) have used selective laser melting, a layer-based solid freeform fabrication technique to create micro cross-flow heat exchangers from stainless steel powder. If used to manufacture heat exchangers, FSC offers the benefit of a single step channel fabrication process. The objectives of this paper are to discuss the channel characteristics for different process parameters and also to prove the stability of the channel along curved profiles, seen commonly in heat exchangers.

Table 2.1 Channel classification (Kandlikar and Grande, 2004)

Conventional channels	$D > 3 \text{ mm}$
Mini-channels	$3 \text{ mm} \geq D > 200 \text{ }\mu\text{m}$
Micro-channels	$200 \text{ }\mu\text{m} \geq D > 10 \text{ }\mu\text{m}$
Transitional channels	$10 \text{ }\mu\text{m} \geq D > 0.1 \text{ }\mu\text{m}$
Transitional micro-channels	$10 \text{ }\mu\text{m} \geq D > 1 \text{ }\mu\text{m}$
Transitional nano-channels	$1 \text{ }\mu\text{m} \geq D > 0.1 \text{ }\mu\text{m}$
Molecular nano-channels	$0.1 \text{ }\mu\text{m} > D$

2.2. EXPERIMENTAL PROCEDURE

Commercial 6061 Al alloy was selected for the study. Three different tools with cylindrical pins and left handed threads were used in this investigation. All the tools had a shoulder diameter of 16 mm, pin diameter of 5 mm, and pin length of 4 mm. Tool 1 had a thread pitch of 1.25 mm, a thread angle of 60° and a depth of cut of 0.4 mm. The equivalent numbers for tool 2 were 1.25 mm, 60° and 1 mm; and for tool 3 were 1.25 mm, 75° and 1.6 mm, respectively. The tools were rotated in the counterclockwise direction as seen from the top of the workpiece. The intent of these runs was to obtain channels with no visible surface defects and of maximum size. The process parameters (the tool rotation rate, traverse speed, and the plunge depth) were varied to obtain this. Optical microscopy was used to measure the size and to characterize the shape of the channels. Force data were acquired using a high frequency data acquisition system connected to the six-axis sensor of the robotic friction stir processing machine.

Mini-tensile specimens of gage length 5mm, width 1 mm and thickness 1 mm were machined at the top of the channel nugget, right above the channels. The specimens

were subjected to tensile loading to determine yield strength, ultimate tensile strength and ductility of the processed material.

2.3. RESULTS AND DISCUSSION

2.3.1. Channel formation. Figure 2.1 shows the cross section of the channel nugget, and depicts clearly the material flow pattern during the process, after the tool has passed the region. The direction of tool rotation is counter clockwise and the traverse direction is into the plane of the paper. To understand the channel formation requires distinguishing among the different regions of the channel cross section. Regions A and B are collectively referred to as the stir zone. Region C is the unprocessed parent material, and region D is the channel. Region E represents the material deposited from the channel nugget region above the original surface of the material, underneath the shoulder. To allow a channel to form, material must be removed from the stir zone. This is accomplished by having a space between the tool shoulder and top surface of the workpiece, and allows the pin features to move the material in this gap. Because of the orientation of the threads on the pin and the direction of tool rotation, the plasticized region at the bottom of the channel is pushed upward on the advancing side (the side where the tool surface velocity vector is opposite to the tool traverse direction). The upward force produced by the threads causes the plasticized material to be pushed upward and deposited by the shoulder on the surface (region E). Region A represents the part of the nugget processed by the pin. The pattern seen in region A depicts the flow path of the material moving from the pin base to the shoulder-workpiece clearance.

The deposition of the material underneath the shoulder results in a downward resultant force on the channel roof behind the pin (trailing side of the tool). Also, due to the shoulder rotation, the material in the upper region of the workpiece is pushed inward and deposited in region B, mainly on the retreating side. An additional layer surrounds the nugget, referred to as a thermo-mechanically affected zone (TMAZ), where the amount of grain refinement is insignificant. TMAZ is unclear in figure 2.1.

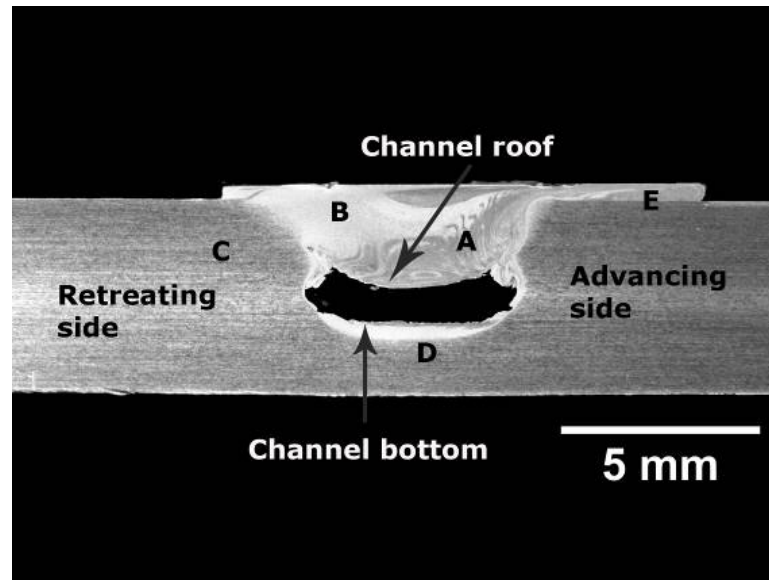


Figure 2.1 Cross-sectional image of a channel showing the different process regions: (A+B) channel nugget, (C) parent material, (D) channel, and (E) material from the channel nugget deposited on the surface.

2.3.2. Channel shape. The shapes of the channels obtained from FSC are closer to an ellipse or oval. The channel shapes usually vary nonlinearly with the process parameters (the tool rotation rate and tool traverse speed). Figure 2.2 shows the variation of the shape of the channel with changing process parameters. As seen in figures 2.2(a) and (b), the channel for a high heat index process condition is visibly well-structured as compared with the channel from the lower heat index process condition. Heat index is a relative term defined as the ratio of the square of the tool rotational rate to the tool traverse speed, and it is used as a representation to differentiate the various processing conditions (Arbegast 2003). The shape variation can be attributed to the volume of material that is displaced from the base of the pin for every rotation of the tool and also the compacting force that is applied on the channel roof during the traverse. For a high heat index run, the volume of material displaced from the pin base is high due to the high tool rotation rate, or alternatively, a low traverse speed. Also, the distance between the roof and base is smaller for the channel created with colder processing parameters. The

shape of the side walls of the channels is influenced by the pin features. The structure of the walls followed the profile of the threads in this study.

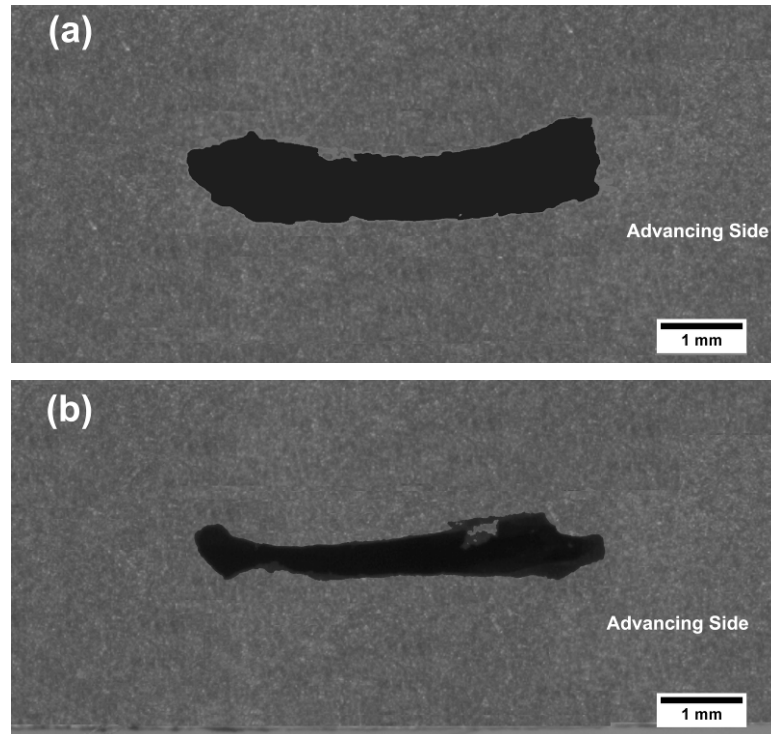


Figure 2.2 Cross section showing the channel shapes at different processing parameters:
 (a) 1100 rpm, 2.11 mm/sec, and (b) 1100 rpm, 2.96 mm/sec.

The forces that act on the tool during processing were logged using a high frequency (~ 2000 Hz) data acquisition system, via a six-axis sensor connected to the friction stir processing machine. Figure 2.3(a) and 2.3(b) shows the process forces acting on the tool during channeling along the x-, y- and z-directions, corresponding to the channels in figure 2.2(a) and 2.2(b). As the tool processes the workpiece, frictional heat is generated at the tool-workpiece interface and subsequently, the material around the pin is preheated and softened. The resistance offered to the pin rotation by the material around the tool reduces due to the softening of the work material. As the processing conditions become hotter, the frictional heat is increased and the process forces acting on

the tool decreases. Similarly, at lower heat indices, the resistance offered to the tool rotation increases.

A closer observation of the process forces and channel shapes show that as the magnitude of the process forces reduces, the shape of the channel is well-structured. It can be inferred that the shape of the channel is influenced by the downward forging force applied by the shoulder on the material in the clearance between the tool and workpiece. The magnitude of the vertical force is low due to high frictional heat. The structural integrity of the channel walls and roof indicates that the force applied by the shoulder is insufficient to cause them to collapse.

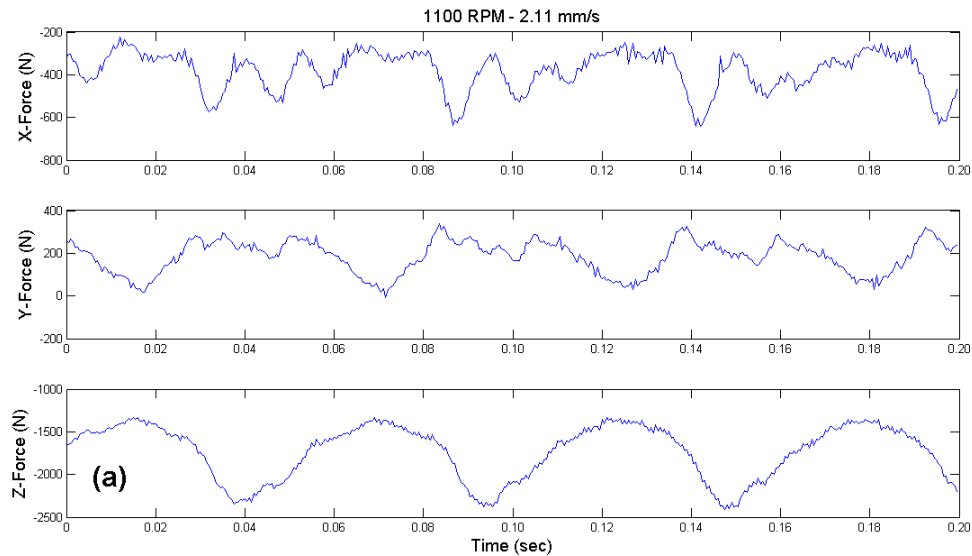


Figure 2.3 Force plots for (a) 1100 rpm and 2.11 mm/sec, and (b) 1100 rpm and 2.96 mm/sec.

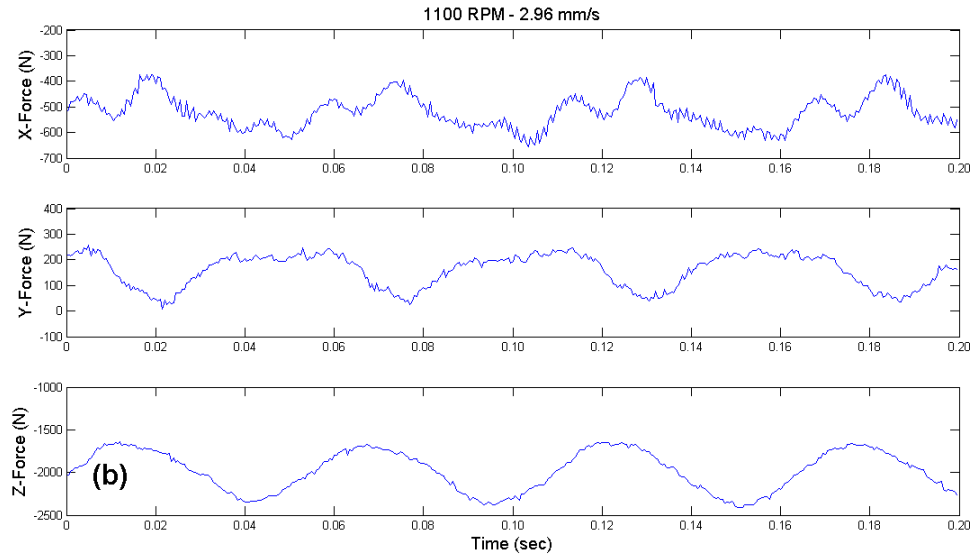


Figure 2.3 (Con't.) Force plots for (a) 1100 rpm and 2.11 mm/sec, and (b) 1100 rpm and 2.96 mm/sec.

2.3.3. Channel size. Figure 2.4 shows the variation of the channel area for different process pitches of the three tools (process pitch is the distance traveled by the tool for one rotation). For any tool, the maximum possible channel area is the maximum volume of material that can be displaced by the pin at any given instance, over a unit length. In this study, tool 3 has the maximum surface area of pin features and theoretically, is expected to generate channels with the largest cross-sectional area followed by tool 2 and tool 1, for a particular plunge depth. As seen from the figure, tool 3 created channels with higher cross-sectional areas for different run parameters.

To further understand the channel size variation with process parameters, the channel area was considered to be directly related to the key process parameters: tool rotational rate and traverse speed at each plunge depth.

$$\text{Area} \propto (\text{tool rotational rate})^{\alpha} \\ \propto (\text{tool traverse speed})^{\beta}$$

$$\text{Area} = K * (\text{tool rotational rate})^{\alpha} * (\text{tool traverse speed})^{\beta}$$

The coefficients α , β and K are unknown and are determined using the method of least squares. The resulting matrix of channel area for different sets of tool rotational rate and

traverse speed are plotted as a contour figure for different plunge depths. The value of coefficient α was negative, and β was positive.

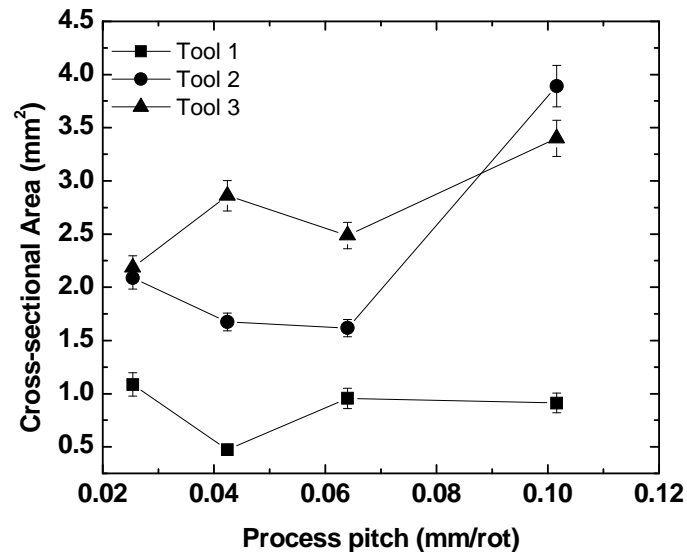


Figure 2.4 Variation of the channel area for different process pitches for the three tools at a depth of 3.0 mm.

Figures 2.5(a) and (b) show the variation of the channel cross-sectional area with the traverse rate and rotational speed of the tool for two different plunge depths. The channel area increases with an increase in the tool traverse speed and a decrease in the tool rotational rate. It was noted that there exists a zone in the process map, where continuous and stable channels were created repeatedly. Defective channels (open channels) or discontinuous channels were observed when the process parameters were outside the optimal process zone. Open channels were created when the processing conditions were extremely colder and this could be due to the inadequate flow of material from the pin base to the shoulder region and the extruded material being insufficient to fill the shoulder-work material clearance. This leads to a situation wherein the shoulder is unable to process the material and distribute it evenly over the top of the channel, which results in the non-closure of the flow arm along the advancing side, and an open and defective

channel. Discontinuous channels were created when the processing parameters were hotter and outside the optimal zone.

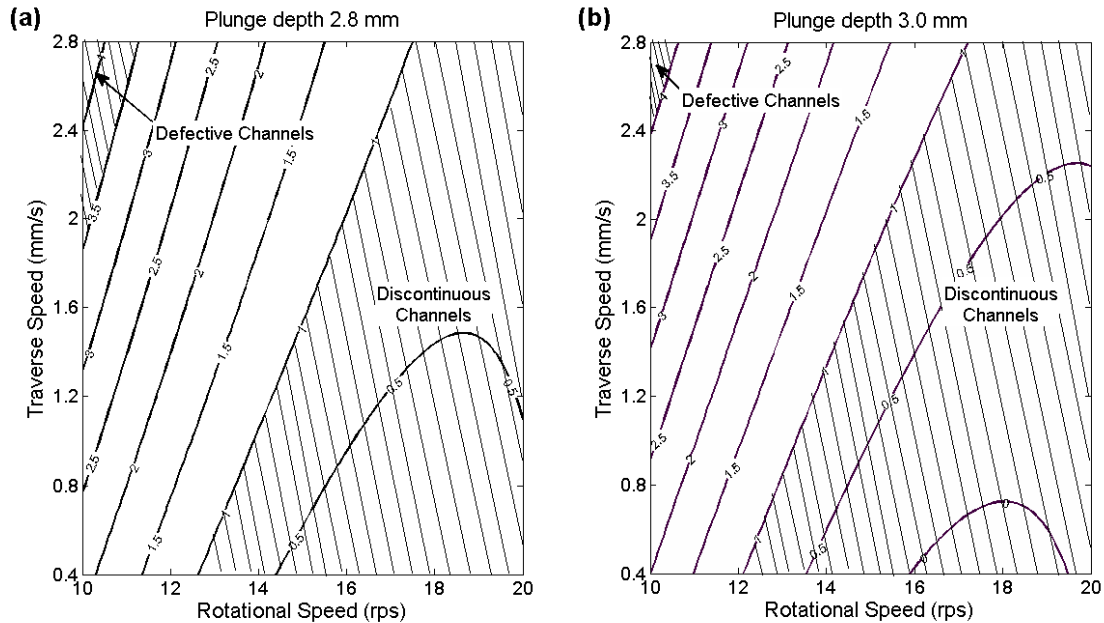


Figure 2.5 Variation of area of the channel with traverse speed and rotational speed at depths of (a) 2.8 mm and (b) 3 mm for the tool 1. The numbers on contour lines represent the area of the channels in mm^2 .

As mentioned in the introduction, hydraulic diameter is the characteristic dimension used in defining channels of non-circular geometries. The variation of the hydraulic diameter of channels obtained using FSC is shown as a function of process pitch in figure 2.6. The values vary from 0.2 mm to 1.2 mm when the clearance between the shoulder and the workpiece is 1 mm. The range of the hydraulic diameter categorizes the channels created by FSC as mini-channels, on the basis of the classification by Kandlikar, 2004.

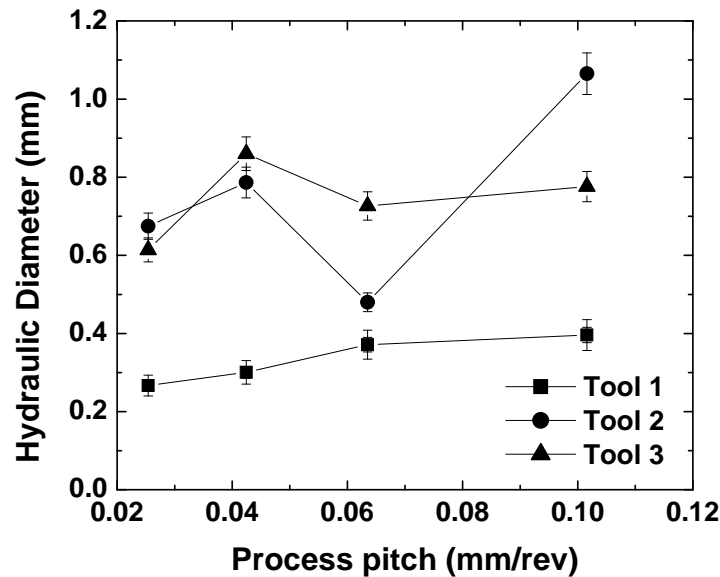


Figure 2.6 Variation of the channel hydraulic diameter for different process pitches for the three tools at a depth of 3.0 mm.

2.3.4. Surface roughness. The surface roughness on the inside surface of any fluid passage is a critical parameter in fluid flow applications. The surface roughness pattern and the roughness dimensions significantly affect the pressure drop inside the flow passages. The channels in FSC are sectioned along the traversing direction, to study the presence of any roughness features.

Figure 2.7(a), (b) and (c) show the longitudinal cross sections of channels produced using different processing parameters. The features of the channels walls vary at the lower and upper surfaces. The bottom of the channel is relatively smooth and flat due to the flat nature of the tool pin base. The upper surface of the channel is rough and undulated and the orientation of this roughness points to the direction of traverse of the tool. The side walls of the channels do not exhibit any roughness features along the length of the channel.

The surface roughness at the upper surface of the channel is uniformly spaced, and the periodicity of the roughness at the top surface matches the amount of material

that is being displaced with each rotation, i.e., the process pitch. In the case of figure 2.7(a), the pitch of the run is calculated to be 0.106 mm/rot. The distance between two successive peaks has been determined to be equal to 0.107 mm. For figure 2.7(b), the pitch of the run is 0.095 mm/rot, and the actual spacing is 0.091 mm. For figure 2.7(c), the pitch is 0.032 mm/rot and the distance between the peaks is 0.033 mm.

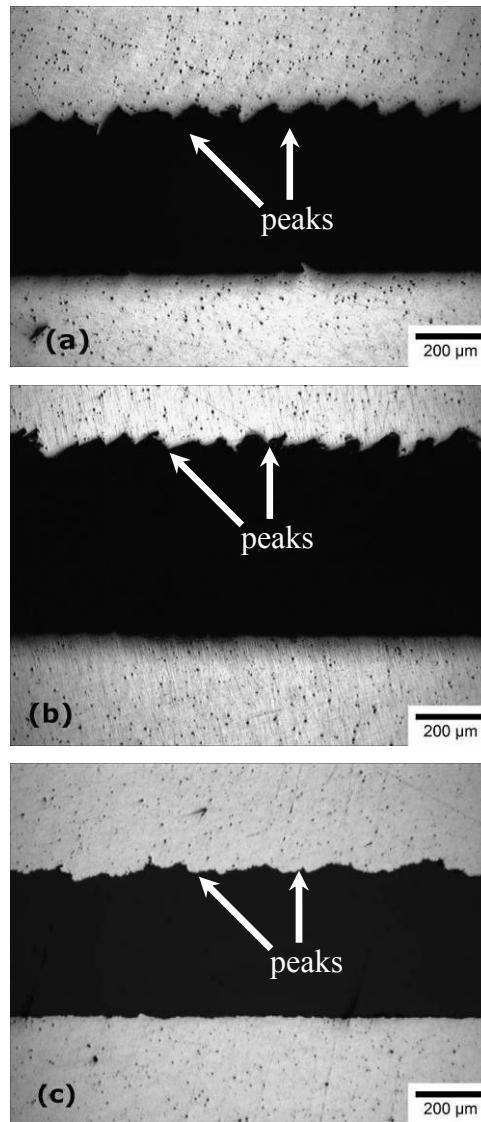


Figure 2.7 Longitudinal cross section of the channel showing the roughness on the roof of the channels. (a) 1200 rpm, 2.11 mm/sec, (b) 800 rpm, 1.27 mm/sec and (c) 800 rpm, 0.42 mm/sec.

2.3.5. Channels along curves. The objective of FSC technique is to create minichannels that can be used in compact heat exchangers. The compact heat exchangers are characterized by the high surface area density values. To have an efficient compact heat exchanger developed using FSC, the process should be capable of generating continuous channels along different profiles. The previous sections dealt with the characterization of channel created along a linear path. In this section, the continuity of channels created along curvature was studied.

Serpentine profiles are one of the most common heat exchanger design patterns used in many industrial applications (Snyder, 1993). The serpentine profile was chosen to maximize the surface area density of a heat exchanger and enhance its performance. Creating serpentine flow passages in heat exchangers is a complex process and typically the pressure losses associated with serpentine profiles are high due to the curvature associated with the profile (Oosthuizen and Austin, 2005). FSC can create channels along serpentine profiles in a time-efficient manner due to the simplicity of the process. To study the continuity of the friction stirred channels, channels were created along curved profiles. The processing parameters used in this study were chosen from the empirical model developed to study the variation of channel size in linear profiles. Continuous channels were produced along both linear and curved profiles for the process parameters chosen from the optimal zone of the empirical model.

Figure 2.8 shows the cross-section of the channels created along two different curved paths using tool 3. The processing conditions and tool rotational direction were maintained the same for the two runs, while the direction of the tool traverse was changed. This was done to vary the position of the advancing side with respect to the traverse path during channeling. The advancing side of the channels in figure 2.8(a) is along the outer curve, while it is on the inner curve in figure 2.8(b). The channels are seen to be continuous in both the cases, but the shape of the channels varies along its length depending on direction of tool traverse. The variation in the channel shapes was more pronounced for profiles with the advancing side on the outer curve. As discussed earlier, material is removed from the base of the pin and moved upward into the clearance region between tool and workpiece on the leading side of the pin. At the trailing side, the shoulder pushes the material from retreating side to the advancing side. This is consistent

with the spread of excess material at the top of the workpiece. The side force exerted by the shoulder at the top surface also results in a downward component. The downward component of the force applied by the shoulder tends to push the material into the void left at the wake of the pin. Depending on the direction of tool traverse, the material is moved either to the inner or outer curves. If the material is moved from the outer curve (advancing side) to the inner curve, the downward force from the shoulder tends to close the channels (figure 2.8(a)). Alternatively, when the material is moved from inner curve (advancing side) to the outer curve, the downward force acting on the material in the clearance between the shoulder and workpiece is insufficient to close the channels. This is shown in figure 2.8(b). Figure 2.9 shows the cross-sectional area of the channels at the different locations and the amount of material deposited in the clearance between the shoulder and parent material for the two cases. The area of the channels for the advancing side in the inner curve is consistently higher than the other case; and the variation in the area along the length is also relatively less.

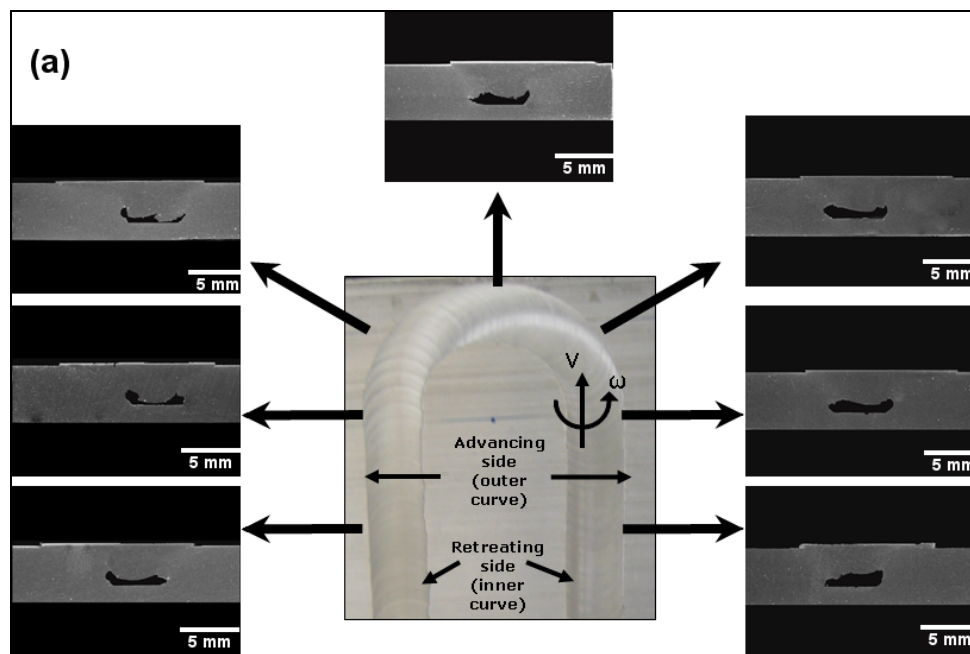


Figure 2.8 Cross sections of the channel at different locations along the curve in a serpentine profile with the advancing side on (a) the outer curve, and (b) the inner curve.

ω represents the tool rotation direction and v represents the traverse direction.

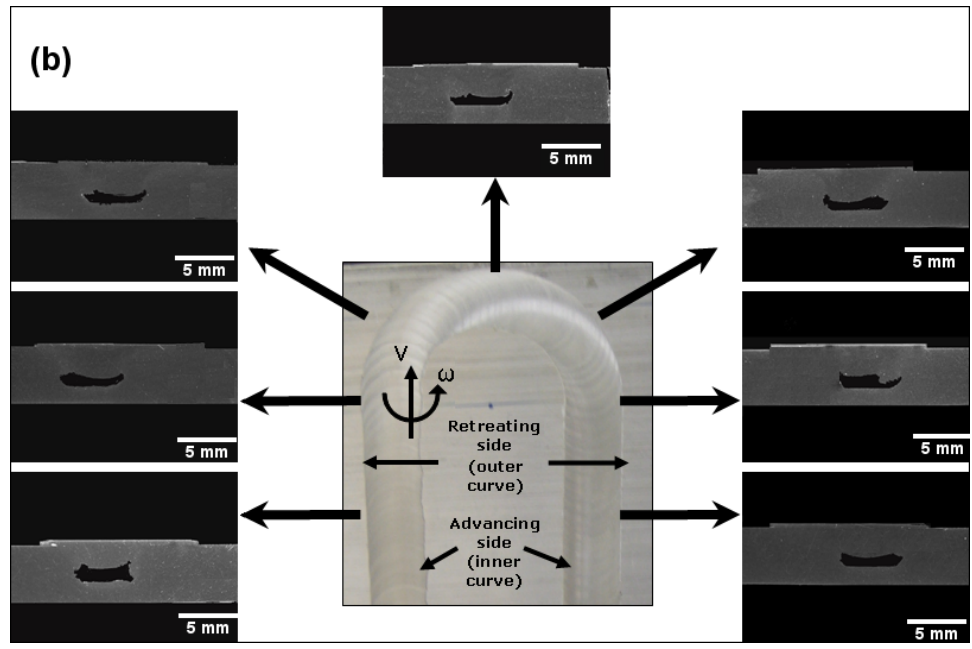


Figure 2.8 (Con't.) Cross sections of the channel at different locations along the curve in a serpentine profile with the advancing side on (a) the outer curve, and (b) the inner curve. ω represents the tool rotation direction and v represents the traverse direction.

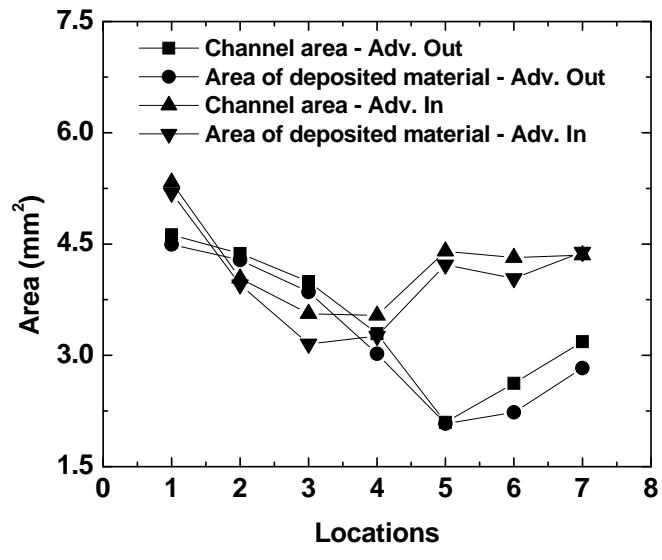


Figure 2.9 Variation of the channel's cross-sectional area and the area of material deposited on top of the parent material along the curve in the serpentine profile.

2.3.6. Mechanical properties. The strength of the material surrounding the channel is important for structural integrity of heat exchangers. The strength values determine the maximum load under which the heat exchangers can operate and also identify the weaker regions where failure can occur. Figures 2.10 (a) and (b) show the strength and ductility of the roof region of processed material in the longitudinal direction. The upper region of the channels had maximum yield strength of 117 MPa and a maximum ultimate tensile strength of 171 MPa, with an elongation up to 12%. Figure 2.11 shows the microhardness profile measured across the transverse cross-section of the channel nuggets created using tool 3. The hardness values are measured at half-way between the channel roof and the workpiece surface. From the results, it can be seen that the hardness values reduce around the center of the channel nugget. The reduction in the strength of the nugget region is expected in friction stir processed material. The softening of the processed region is caused by coarsening and dissolution of strengthening precipitates during the thermal cycle of the FSP (Mahoney et al., 1998).

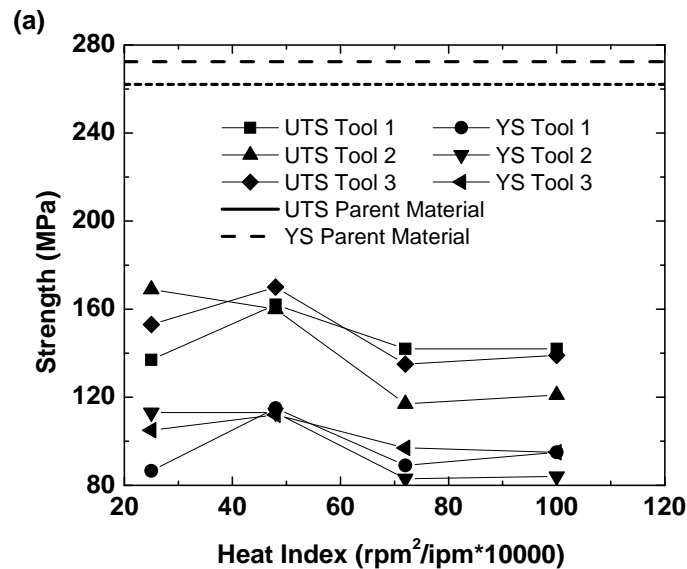


Figure 2.10 Strength of material on the roof of the channel along the longitudinal direction, (b) elongation of material on the roof of the channel along the longitudinal direction.

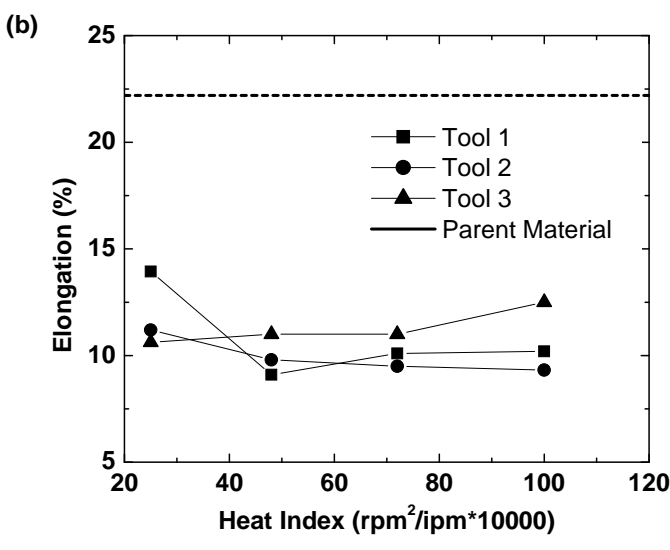


Figure 2.10 (Con't.) Strength of material on the roof of the channel along the longitudinal direction, (b) elongation of material on the roof of the channel along the longitudinal direction.

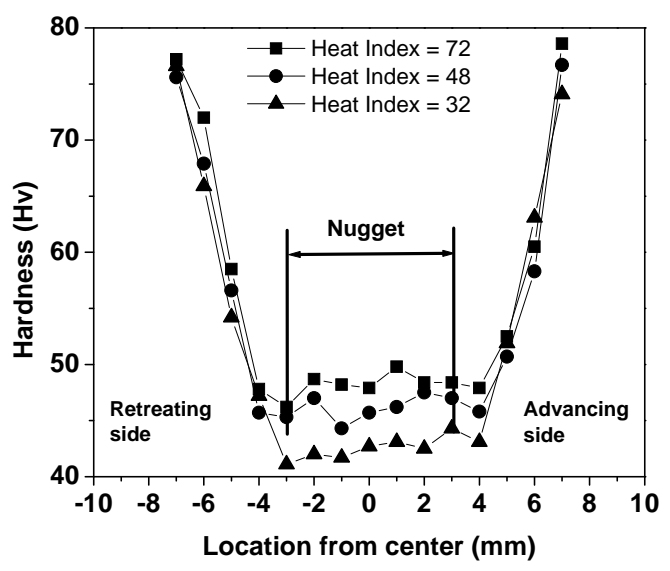


Figure 2.11 Microhardness profile across the channel nugget processed by tool 3 for different heat indices.

2.4. FINISHING PROCESS

The channels created using FSC technique require minimal finishing. Excess material on the top surface of the workpiece can be milled and a smooth surface finish can be obtained.

2.5. CONCLUSION

Continuous and integral channels were achieved along linear and curved profiles. The channel shape during FSC can be modified by changing the processing parameters and thereby control the volume of material getting displaced from the pin base. The channel size increases with an increase in the traverse speed and decrease in the rotational rate. The hydraulic diameters of the channels vary from 0.2 mm to 1.2 mm, classifying them as minichannels. There is a periodicity of roughness peaks in the roof region of the channels, which match with the process pitch. The roughness pattern is expected to be significant in the pressure drop in heat exchanger applications.

2.6. ACKNOWLEDGMENT

The authors gratefully acknowledge the support for this research from the National Science Foundation through grant DMI-0523022.

2.7. REFERENCES

- Arbegast, W., 2003. Modeling friction stir joining as a metal working process. In: Hot deformation of aluminum alloys III, TMS, San Diego, CA, pp. 313-327.
- Brandner, J.J., Anurjew, E., Bohn, L., Hansjosten, E., Henning, T., Schygulla, U., Wenka, A., Schubert, K., 2006. Concepts and realization of microstructure heat exchangers for enhanced heat transfer, *Exp. Therm Fluid Sci.*, 30, pp. 801-809.
- Hrnjak, P, Tu, X, 2007. Single phase pressure drop in microchannels. *Int. J. Heat Fluid Flow*, 28, pp. 2–14.

- Kandlikar, S.G., Grande, W.J., 2004. Evolution of microchannel flow passages - thermohydraulic performance and fabrication technology, *Heat Transfer Eng.*, 24, pp. 3-17.
- Li, Z., Tao, W-Q., He, Y-L., 2006. A numerical study of laminar convective heat transfer in microchannel with non-circular cross-section, *Int. J. of Thermal Sciences*, 45, pp. 1140-1148.
- Mahoney, M. W., Rhodes, C. G., Flintoff, J. G., Spurling, R. A., Bingel, W. H., 1998. Properties of friction-stir-welded 7075 T651 aluminum, *Metall. Mater. Trans. A*, 29A, 1955-1964.
- Mishra, R.S., Ma, Z.Y., 2005. Friction stir welding and processing, *Mater. Sci. Eng.*, R, 50, 1-78.
- Mishra, R. S., 2005. Integral channels in metal components, US Patent 6,923,362.
- Mehendale, S.S., Jacobi, A.M., Shah, R.K., 2000. Fluid flow and heat transfer at micro- and meso-scales with application to heat exchanger design, *App. Mech. Rev.*, 53, pp. 175-193.
- Oosthuizen, P. H., Austin, M., 2005. Channel-to-channel pressure differences in serpentine minichannel flow systems, *Microscale Therm. Eng.*, 9, pp. 49-61.
- Reynolds, A. P., 2007. Microstructure development in aluminum alloy friction stir welds. In: Mishra, R.S., Mahoney, W.M. (Eds.), *Friction Stir Welding and Processing*, ASM International, pp. 51-70.
- Shah, R.K., Sekulic, D. P., 2003. *Fundamentals of heat exchanger design*, first ed, Wiley, pp. 1-73.
- Snyder, B., Li, K.T., Wirtz, R.A., 1993. Heat transfer enhancement in a serpentine channel, *Int. J. Heat Mass Transfer*, 36, pp. 2965-2976.
- Thomas, W.M., Nicholas, E.D., Needham, J.C., Murch, M.G., Templesmith, P., Dawes, C.J., 1991. G. B. Patent Application No, 9125978.8.
- Tsopanos, S., Sutcliffe, C.J., Owen, I., 2005. The manufacture of micro cross-flow heat exchangers by selective laser melting. In: *Proceedings of Fifth International Conference*

on Enhanced, Compact and Ultra-Compact Heat Exchangers: Science, Engineering and Technology, pp. 410-417.

Wadekar, V.V., 2005. Heat exchangers in process industry and mini- and microscale heat transfer. In: Proceedings of Fifth International Conference on Enhanced, Compact and Ultra-Compact Heat Exchangers: Science, Engineering and Technology, pp. 318 – 325.

Wu, H.Y., Cheng, P., 2003. Friction factors in smooth trapezoidal silicon microchannels with different aspect ratios, *Int. J. Heat Mass Transfer*, 46, pp. 2519–2525.

3. PROCESS FORCES DURING FRICTION STIR CHANNELING IN AN ALUMINUM ALLOY

N. Balasubramanian¹, R. S. Mishra^{2,‡}, K. Krishnamurthy¹

¹ Mechanical and Aerospace Engineering, Missouri University of Science and Technology, Rolla, MO 65409, USA

² Center for Friction Stir Processing, Materials Science and Engineering Department, Missouri University of Science and Technology, Rolla, MO 65409, USA

ABSTRACT

Friction stir channeling (FSC) is an innovative technique for manufacturing continuous channels that can be applied in heat exchanging applications. An understanding of the material flow behavior during FSC is essential to produce consistently stable and continuous channels. Analysis of the relationships between the process input parameters and the forces associated with friction stir processing (FSP) is emerging as an efficient technique to study the material flow patterns. In this study, channels were fabricated in Al6061-T6 alloy using FSC and the process forces were measured using a high frequency data acquisition system. Polar plots of the net resultant force acting on the tools are plotted and correlated with the process parameters and channel features.

Keywords: friction stir channeling, friction stir processing, process forces, material flow, aluminum alloys

3.1. INTRODUCTION

Friction stir processing is an adaptation of friction stir welding (FSW) that builds upon some of the unique features of FSW to develop new processes [1]. FSP techniques

[‡] Corresponding author. Tel.: +1-573-341-6361; e-mail: rsmishra@mst.edu

utilize one or more of the following features: the very fine grain size in the stirred region, the extensive plastic flow of material, the low amount of heat generated, the absence of flaws and pores, and the mechanical mixing of the surface and subsurface layers [2]. During FSW a defect referred to as a “wormhole” is generated if the processing parameters are not optimal. Arbegast [3] has discussed the formation of different defects during FSW, including wormhole generation. The study presents a model based on the flow partition deformational zones for defect formation. The occurrence of wormholes in the FSW nugget has been attributed to flow defects because of the non-optimal processing conditions or geometry of the tool features. The model applies the principle of mass balance to address void formation in the nugget. FSC technique is established on the concept of converting this defect formation into a continuous and stable channel.

FSC is a non-traditional technique of creating continuous, integral channels in a monolithic plate in a single pass that is proposed as a method of manufacturing compact mini-channel heat exchanging devices [4]. FSC relies on the frictional heat generated between the tool material and the metal workpiece to soften and deform the material to facilitate the creation of a continuous channel. Mishra [4] has achieved a continuous hole in a single plate by selecting the optimal processing parameters and reversing the material flow pattern of FSW. Balasubramanian et al. [5] have discussed using the concept of FSC to create continuous channels inside monolithic plates. The channel formation process has been dealt in detail and the channel is characterized for its size, shape and internal features. This work also examined the continuity of the channels along linear and curved profiles. The two main aspects of FSC process can be summarized as follows:

1. a profiled FSP tool is rotated such that the material flow is upwards towards the tool shoulder, and
2. an initial clearance is provided between the shoulder and the workpiece, where the material from the base of the pin is deposited.

Figure 3.1 shows an example of channel achieved using the FSC technique. The cross section of the channel nugget and the material flow pattern during the process can be noted. To allow a channel to form, material must be removed from the base of the pin in the nugget. A combination of the orientation of the threads on the pin and the direction of tool rotation results in the displacement of material from the pin base and it gets

pushed into a clearance region between the tool shoulder and top surface of the workpiece. The flow arm is along the advancing side of the pin and the displaced material is spread over the parent material by the rotation of the shoulder with a bias towards the advancing side.

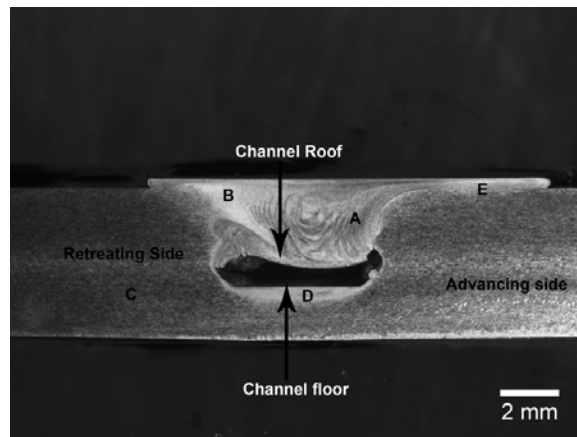


Figure 3.1 Cross-sectional image of a channel.

Researchers have focused on understanding the flow and consolidation of material during FSW/P using both experimental and numerical techniques. Flow visualization studies [6, 7] and numerical analyses [8, 9] have been performed in an effort to understand the material flow pattern. While the experimental techniques to visualize the material flow pattern provide a post-mortem analysis of the process, the computational models are constrained by two different sets of requirements, (a) relevant values for materials and coupling properties, and (b) powerful computational resources and time. To overcome the inherent disadvantages of these methods, focus is shifting towards analyzing the force signatures created by varying the process parameters during FSW/P. Force analysis has been widely used to study the working mechanism of conventional machining process like milling and drilling. Using force patterns to analyze material flow behavior is a relatively new development in FSW/P. Hattingh et al. [10] have studied the relationship between tool shape, process parameters, and microstructure using force foot

print diagrams. They developed plots to show the force vector experienced by the tool during each revolution. Long et al. [11] studied the effects of material properties and process parameters on traverse forces and weld defect formation (via material flow patterns) using fluid dynamics simulation. Yan et al. [12] studied the relationship between the periodicity of process parameters and that of the micro- and meso-structural banding in FSW. The oscillation of FSW parameters during baseline experiments without welding and during a series of FSW of AA2524 and AA2024 aluminum alloys were measured and analyzed for the banded structures in all the welds. The measured band spacing was correlated with the oscillation period of process forces F_x and F_z exerted on and by the welding tool. Arbegast [13] has experimentally demonstrated the change in process forces due to clamping locations, welding direction, crossing over pre-existing FSW and change in the process parameters (rotation rate and traverse speed). A multi-axial transducer capable of capturing the process force foot print that can be used to measure the energy input to welding was developed by Blignaut et al. [14]. Hattingh et al. [15] have analyzed the force foot prints to study the influence of tool geometry on FSW process parameters and on weld tensile strength and thereby optimize the tool design to produce welds with 97 % of the parent plate tensile strength in Al 5083-H321 alloy. Balasubramanian et al. [16] have investigated the effect of process forces during FSP of cast and wrought aluminum alloys. Polar plots of the net resultant forces acting on the tool during processing were used to understand the presence or absence of defects in the nugget region. Studying the process forces associated with the plastic flow around the pin is critical to the understanding of the FSC technique. In this research, the polar plots of the net resultant traverse forces and the force signature was evaluated to understand the material flow pattern during channeling.

3.2. EXPERIMENTAL PROCEDURE

Friction stir channels were fabricated on 5 mm thick plates of Al6061-T6. The nominal composition (by % weight) of Al6061-T6 is Al-1.0Mg-0.6Si-0.30Cu-0.20Cr. The experimental setup consists of an IRB-940 Tricept 6-axis robot with three non-parallel telescopic translational joints and three rotational joints. The robot is fitted with a friction stir welding head from Friction Stir Link, Inc., that provides the rotational motion

to the tool. The friction stir spindle assembly consists of a rotational axis driven by a servo motor that can speed up to 3000 rpm. The load rating of the spindle is 9 kN along the tool axis and 4.5 kN in the radial direction. A JR3 multi-axis force sensor attached to the spindle head can determine the loading on the tool by measuring the forces along three orthogonal axes and moments about each of the three axes. The rated loads for the sensor are 6 kN in x and y directions and 12 kN in the z direction and the rated moments are 1150 Nm about all the three axes. During processing, the process forces and moments were logged at a frequency of 2000 Hz using a high frequency data acquisition system.

To study the influence of processing conditions, and pin profiles on the nugget characteristics and the process forces, the plates were friction stir processed using different processing conditions by varying the tool rotation rate and traverse speed, and with different pin geometries. The dimensions and features of the three tools used in this study are given in Table 3.1 and the processing conditions are listed in Table 3.2. The pin was penetrated to a depth of 3.2 mm (providing a clearance of 0.8 mm between the shoulder and the workpiece). The tool tilt angle was 0° for all the runs. The processed materials were then sectioned, and polished to study the nugget features using an optical microscope.

Table 3.1 Dimensions of the friction stir channeling tools

Tool	Shoulder Diameter (mm)	Pin Length (mm)	Pin Diameter (mm)	Thread Profile	Thread Pitch (mm)	Thread Angle (degrees)	Depth of Cut of the Threads (mm)
FSC11	16	4	5	LHT	1.25	60	0.2
FSC12	16	4	5	LHT	1.25	60	0.5
FSC13	16	4	5	LHT	1.25	75	0.8

Table 3.2 Processing parameters

Process ID	Tool Rotation Rate (rpm)	Tool Traverse Speed (mm/sec)
1	1100	2.17
2	1100	2.96
3	1200	2.17
4	1200	2.96


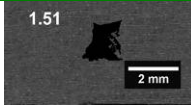
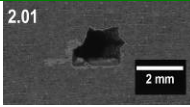

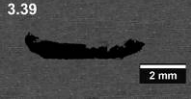


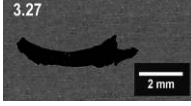
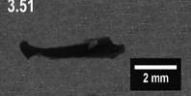
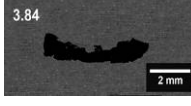
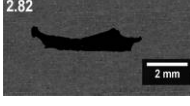

3.3. RESULTS AND DISCUSSION

3.3.1. Macrostructure. The macrostructure of the friction stirred channels were studied using optical microscope to observe the channel shape, size and continuity. The macrostructure of the processed region and the observed channel features (shape and cross-sectional area) as measured from the macroscopic images are presented in this section. Table 3.3 shows the nugget features for the material processed with tools FSC11, FSC12 and FSC13. Figure 3.2 is a plot of the variation of the cross-sectional area of the channels as a function of pseudo-heat index [17]. The pseudo-heat index is a relative term defined as the ratio of the square of the tool rotational rate to the tool traverse speed, and it is used as a representation to differentiate the various processing conditions. From the macroscopic images, it can be observed that the cross-sectional area of the channels is larger and the shape is well-structured when processed with the tools FSC12 and FSC13 as compared to FSC11.

During FSC, a combination of the orientation of the threads on the pin and the direction of tool rotation results in displacing the material from the base of the pin to the clearance between the shoulder and the workpiece. The size of the channels created by FSC technique is relative to the volume of material that can be displaced by these threads. During each rotation of the tool, a shear deformation zone is created at the pin-workpiece interface. The material is sheared from the parent material and displaced from the advancing side to the retreating side of the tool. When there is a loss in the volume of material that is displaced by the tool rotation, voids occur. The structure and size of these

voids are dependent upon the processing conditions and the geometry of the tool features. Among the tools used in this study, the threads in FSC13 have a larger depth-of-cut and a higher thread angle as compared to the other two tools. The thread angle in FSC12 is the same as in FSC11, but with a larger depth-of-cut. This dissimilarity in the dimensions of pin features results in the variation in size of channels created by the three tools. It is also noted that with an increase in the heat index of the process parameters, the channel area decreases. This reduction in channel area is in conjunction with the observations made by Balasubramanian et al. [4] for different process parameter combinations. However, all the channels were found to be stable and continuous along the length of the process. There was no macroscopic variation in the shape and size of the channels over the process length for the same process parameter combination. From the analysis of the macrostructure, it is clear that the channels formation in the nugget zone is a function of the tool profile and process parameters.

Table 3.3 Channel features for Al6061-T6 processed using FSC. The numbers indicate the area of the channel in mm^2 .

Tool ID	1100 rpm	1100 rpm	1200 rpm	1200 rpm
	2.11 mm/sec	2.96 mm/sec	2.11 mm/sec	2.96 mm/sec
FSC 11	2.36 	1.51 	2.01 	1.57 
FSC 12	3.39 	3.72 	2.96 	3.27 
FSC 13	3.51 	3.84 	2.82 	3.67 

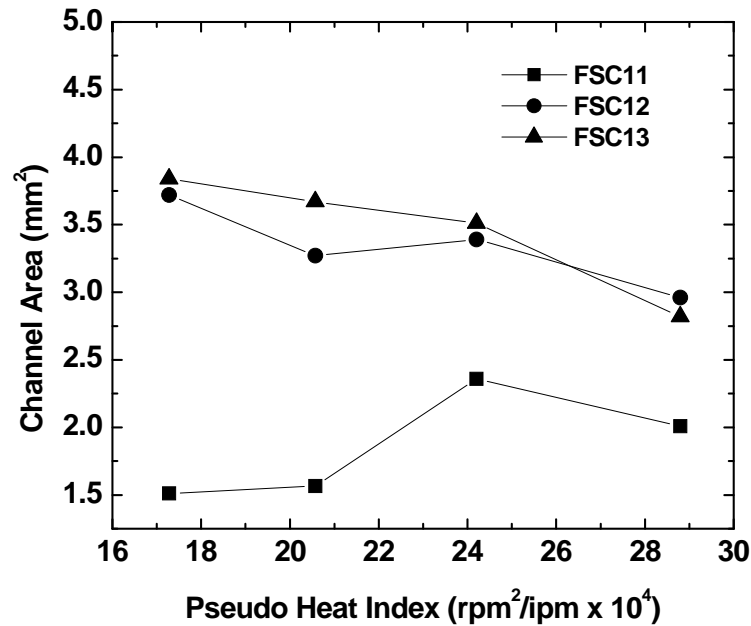


Figure 3.2 Plot showing the variation of the cross-sectional area of the channels for the three tools, as a function of the pseudo heat index.

3.3.2. Polar Plots. Figure 3.3 shows a schematic of the FSC process and the co-ordinate system of the forces. The system can be visualized as a left-handed co-ordinate system where the x-force is the load acting on the pin surface normal to the direction of traverse, the y-force is the horizontal force acting along the transverse direction and is perpendicular to x-force, and the z-force is the vertical force acting on the base of the pin surface. Similarly, the x-, y- and z-moments act along the x-, y-, and the z- axes.

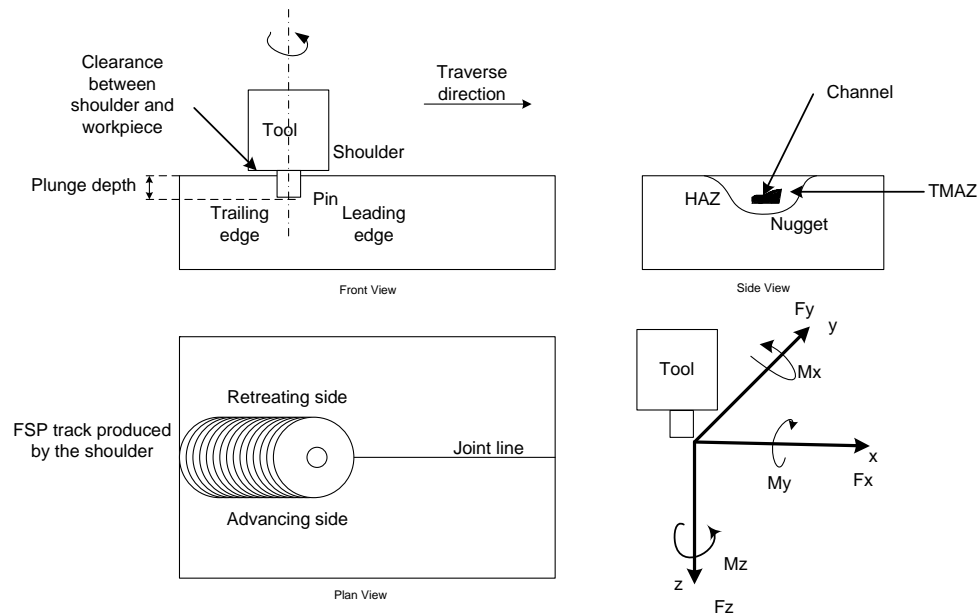


Figure 3.3 A schematic representation of friction stir channeling and co-ordinate system of the FSC forces measured using the high-frequency data acquisition.

At any instant during the channeling process, forces are imparted on the pin by the material flowing around it. The net effect of these forces moves the pin elastically from its center line. During traversing, the pin comes in contact with the new material in front of it along its leading edge, which imparts a compressive force on the pin surface. As the tool rotates, material is displaced from the base of the pin by plastic deformation into the clearance between the shoulder and the workpiece. The material flow arm extends from the channel base into the shoulder clearance along the advancing side. As the material builds up in the clearance, the shoulder surface processes the material and moves it from the advancing side to the region between the retreating side and trailing edge. The shoulder also applies a downward forging force on the material, thereby pushing it into the void left at the pin's wake. The channel roof is thus formed as a result of the consolidation of the material flowing from the pin base to the shoulder clearance and the downward forging force applied by the shoulder. This material in the trailing edge applies a compressive force on the pin that would be relatively lower in magnitude

compared to the force applied by the material at the front of the pin. The resultant force acting along the x-y coordinate frame is the net effect of the forces applied by the new material from the front of the pin and the processed material from its rear. This effect is visualized clearly when the resultant of x and y forces are plotted as polar plots. Since x- and y-forces are perpendicular to each other, the magnitude and the angle of the resultant are given by equations 1 and 2, respectively.

$$F_r = \sqrt{F_x^2 + F_y^2} \quad (1)$$

$$\theta = \tan^{-1} \left(\frac{F_y}{F_x} \right) \quad (2)$$

where, F_r is the magnitude of the net resultant force and θ is the angle between the x-axis and the resultant. The magnitude and location of the resultant force can help understand the material flow patterns. Negative force values indicate compressive loading on the tool and positive values indicate tensile loading.

Figure 3.4 shows the polar plots of the net resultant force acting on the tool FSC11 in Al6061-T6 for one complete rotation of the tool. Figures 3.5 and 3.6 show the polar plots of the resultant force acting on tools FSC12 and FSC13 for different processing parameters. A closer investigation of the polar plots for the three tools (Figures 3.4, 3.5, and 3.6) along with the plot of variation of the size of channels (Figure 3.2) shows the following features:

- *When the processing parameters are hotter the magnitude of the net resultant force tends to be lower.* At higher heat indices, the material ahead of the pin is pre-heated and softened due to frictional heat that is generated at the tool-workpiece interface. The force required by the tool to shear the material is reduced due to softening. This leads to a decrease in the net resultant force acting on the pin during the processing of the material.

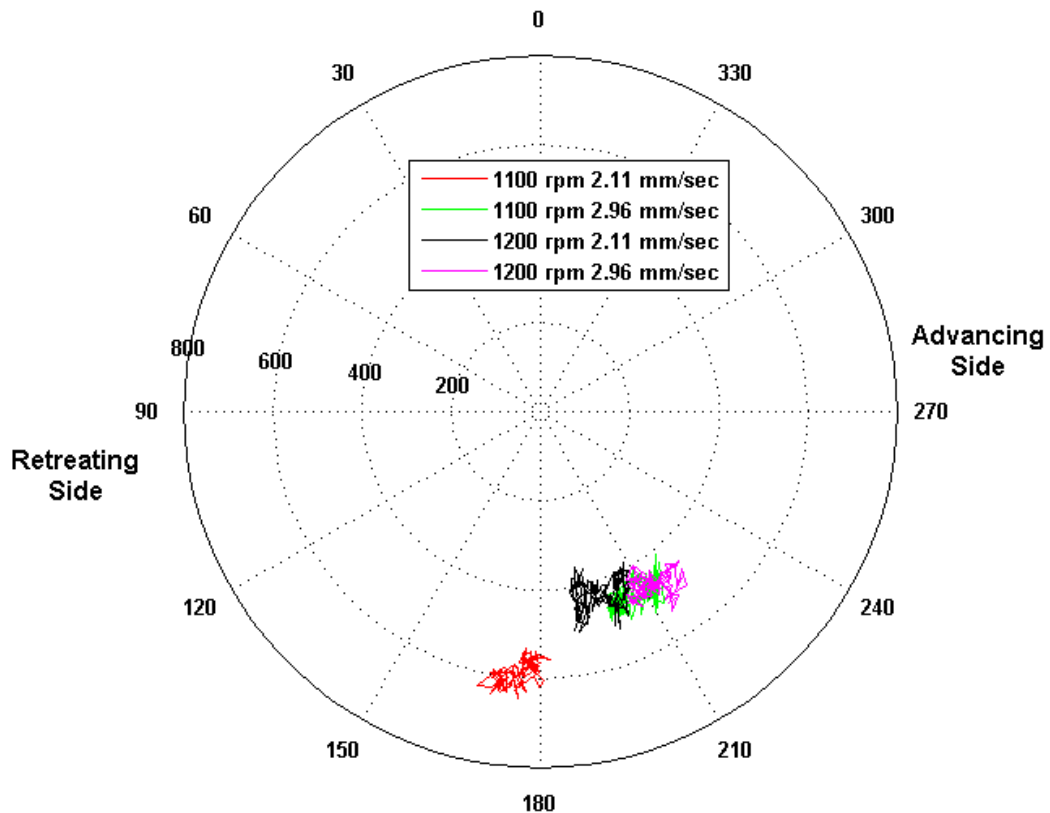


Figure 3.4 Polar plots of the resultant forces (units - N) during FSC of Al6061-T6 using FSC11.

- When channels exist in the nugget region, the net resultant force is positioned at the trailing side of the tool's traverse path. As the tool rotates, material is removed from the base of the pin and moved along the advancing side-leading edge into the clearance between the shoulder and workpiece. This material is spread by the shoulder over the parent material. As it spreads the material, the shoulder applies a vertical downward force (F_z) on this material and when this force is high, the material is pushed into the void. This leads to a closure of the channels or creation of partial channels. As the material closes the void, it applies a force on the pin surface from the region between the retreating side and trailing edge, pushing the pin towards the advancing side. The movement of the net resultant force closer to the advancing side*

is clearly seen in the polar plots. Also, Figure 3.2 shows that as the force moves closer to the advancing side, the channel area drops.

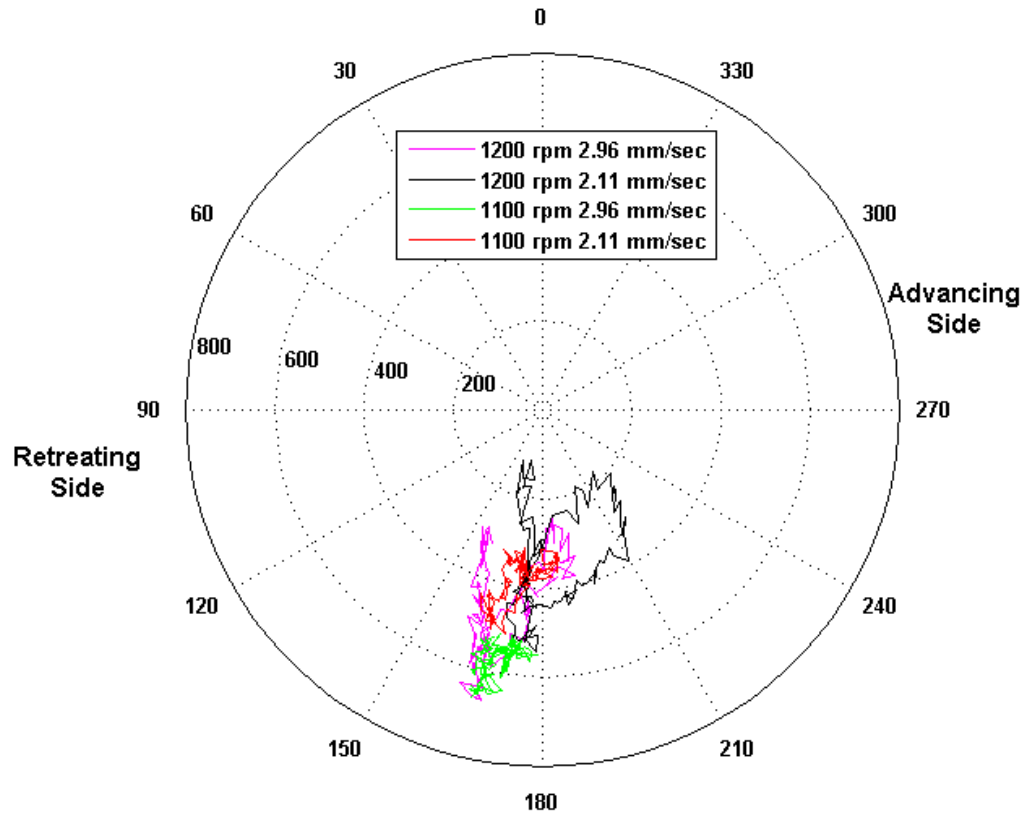


Figure 3.5 Polar plots of the resultant forces (units - N) during FSC of Al6061-T6 using FSC12.

- *Partially formed channels are created when there is a lack of material flow from the pin to the shoulder-workpiece clearance.* This is seen for the channels created using the FSC11 tool. As discussed in the previous section, the volume of material that a tool can help displace during each rotation depends on to the geometrical dimensions of the pin features. In the material processed by FSC11, the volume of the material displaced by the tool is less and hence, the channel is smaller compared to the other tools.

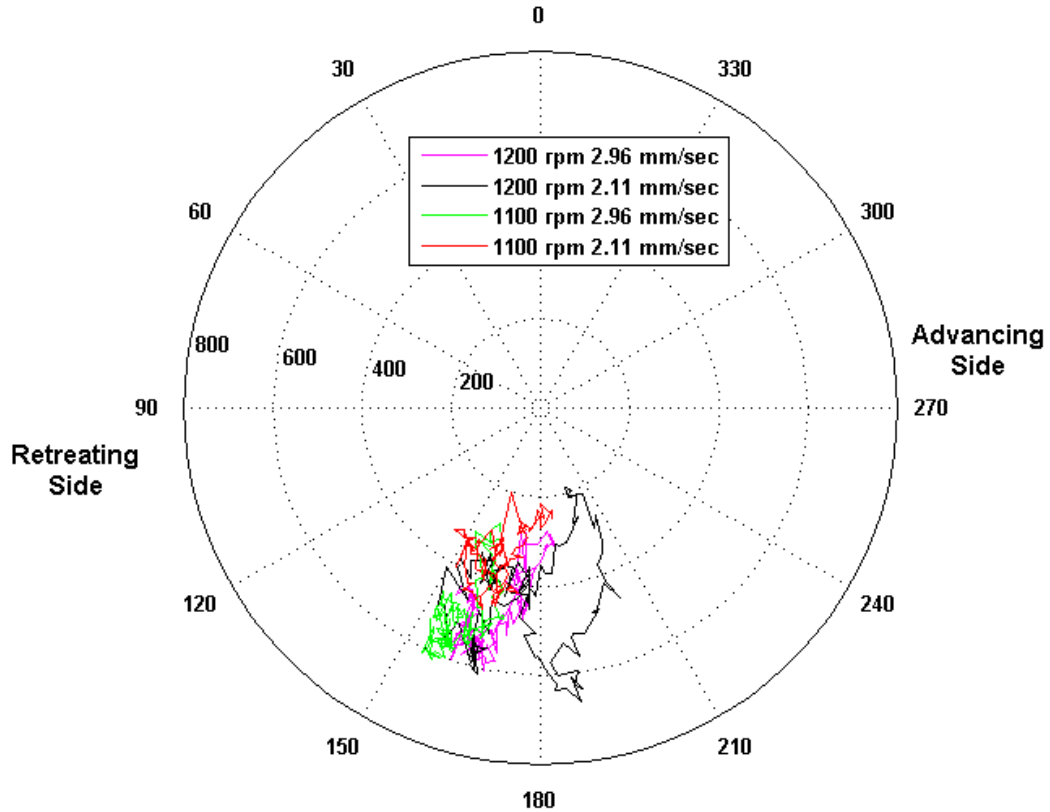


Figure 3.6 Polar plots of the resultant forces (units - N) during FSC of Al6061-T6 using FSC13.

- The spread of the net resultant force is larger for hotter runs as compared to the colder runs.* This is likely to be due to lower flow stress of the material at higher temperatures. All friction stir welding machines have some runout. As the material is softened, it is easier for the pin to be displaced from its traverse path due to spindle runout [6, 12]. When the material flows from the advancing side to the retreating side, the pin is displaced from its center line. This is shown by the large area covered by the spread of the resultant force. When the spread of the force profile is larger, it is noted that the channel has a well-defined shape. The base of the channel in these runs is of the same size as the pin diameter as seen in the nuggets processed using the tools FSC12 and FSC13. For the channels processed with FSC11, the spread of the net

resultant force is quite compact. The macroscopic images of these channels show that width of the channel base is not the same as the pin diameter.

3.3.3. Force Signature. Figure 3.7 shows the profile of the x-, y- and z- forces acting on tool FSC12 at 1200 rpm and 2.11 mm/sec. The cross-sectional view of the channel is inset in the figure. The shaded region in the picture is the force profile for one complete rotation of the tool. The orientation of force signs is given in Figure 3.3. Figure 3.8 is the profile of the forces acting on tool FSC12 at 1200 rpm and 2.96 mm/sec.

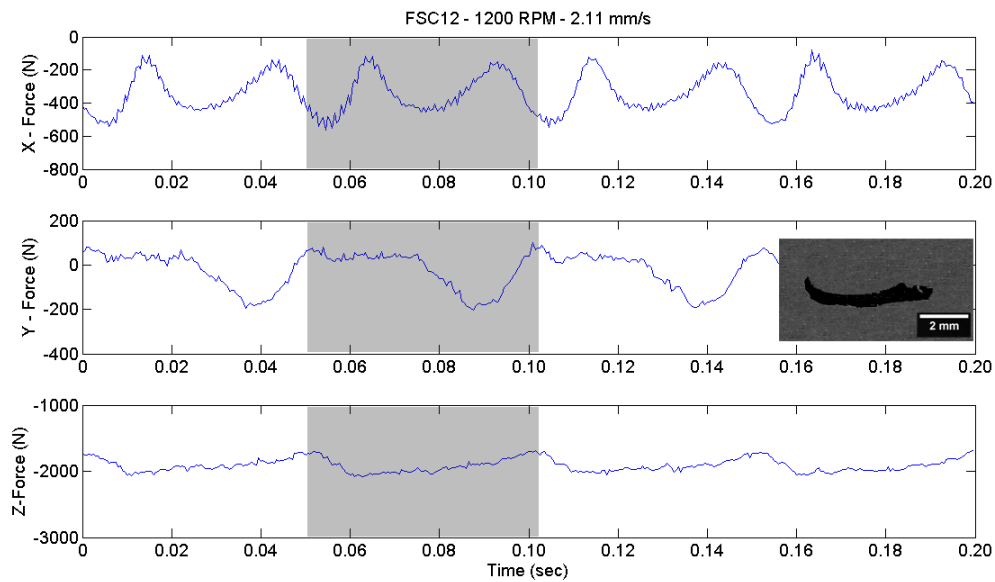


Figure 3.7 Force plots for 1200 rpm and 2.11 mm/sec using FSC12 with an inset of the channel. Shaded region shows the force profile for one complete rotation of the tool.

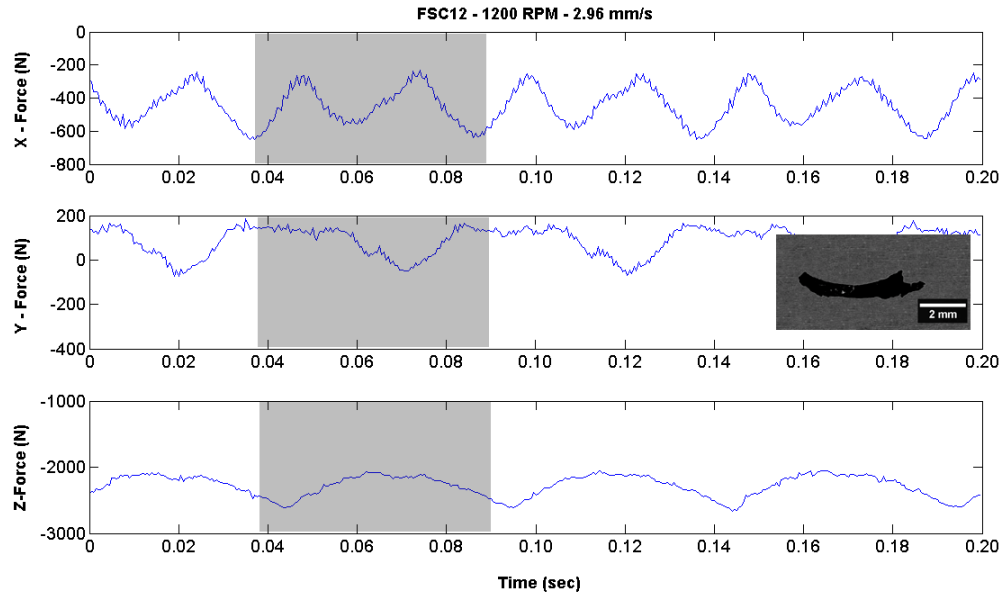


Figure 3.8 Force plots for 1200 rpm and 2.96 mm/sec using FSC12 with an inset of the channel. Shaded region shows the force profile for one complete rotation of the tool.

There is a periodic variation to the force patterns along all three directions. The periodicity of the variations was calculated to be equal to the time taken for one complete rotation of the tool. Also, the magnitude and amplitude of variation of these forces is different for both processing conditions. Z-force is always negative as the tool experiences compressive force. X-force values are negative, indicating that tool is being pushed to the trailing edge by the moving material. Oscillation of y-force in positive and negative values indicates that pin experiences push to the advancing as well as the retreating side within one revolution. Reynolds [6] has shown that these variations are not just a result of the tool rotation and traverse, but also due to the tool runout. It can be noticed that during each rotation, the x-, y-, and z- forces cycle from a higher magnitude to a lower magnitude and back. This amplitude is a pointer to the variations in contact conditions and movement of material over the course of each rotation. But the number of cycles for each revolution varies for the three axes. There is one cyclic raise and drop for the z-force and y-force, while there are two cycles for each revolution for the x-force. During each revolution of the tool, the material is deformed and displaced from the pin base and flows vertically upwards to the shoulder-workpiece clearance. This flow arm

extends along the advancing side-leading edge. The pin-processed material is then acted upon by the shoulder surface that moves it from the advancing side to the retreating side. As the shoulder spreads this material from the leading edge to the retreating side, it applies a downward forging force on the material. This is clearly seen in the increase of F_z in the force plots. The forging force then reduces gradually as the tool moves from the retreating side to the advancing side, where it meets the new load of pin-processed material. It can be observed that forces along the y-direction have one cycle per revolution. The magnitude of force changes rapidly from low to high and back and then remains low for the rest of the cycle. At the instant when the value of F_y is high, F_z has a decreasing slope. But in the same time frame, there are two peaks and troughs in the x-direction. Yan et al. [12] have reported the presence of one cycle in the periodicity of F_x and F_z within each tool revolution and concluded that the tool and work motion interaction leads to these oscillations. The geometry of the pin features can significantly affect the volume of material sticking to the surface over each rotation. Also, tool runout during processing can affect the magnitude and amplitude of the forces acting on the tool.

Figure 3.9 is the SEM of the roof of the channel for the material processed with FSC12 at 1100 rpm and 2.96 mm/sec. Figure 3.10 shows the forces acting of FSC12 for the same parameters. Distinct bands of material flow and deposition can be observed on the roof. The distance between these bands matches the pitch of the run (distance of tool advance per rotation). These deposits hang along the roof of the channels. They are formed from the material that is pushed down by the shoulder during each rotation. Three to four minor bands that are evenly spaced are seen between the major bands. When overlaid against the force profile, these bands match well against the major peaks and drops in the x-force. This is shown clearly in figure 3.10. This is in concurrence with the findings by Yan et al. [12] that the force cycles matches with the processing bands seen in the microstructure of the friction stir nugget.

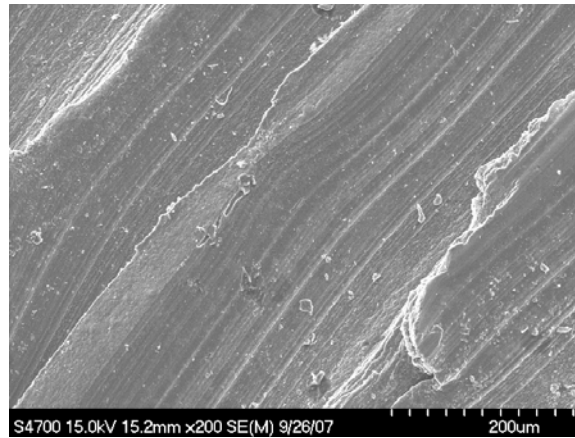


Figure 3.9 SEM of the material on the roof of the channel processed at 1100 rpm and 2.96 mm/sec using FSC12.

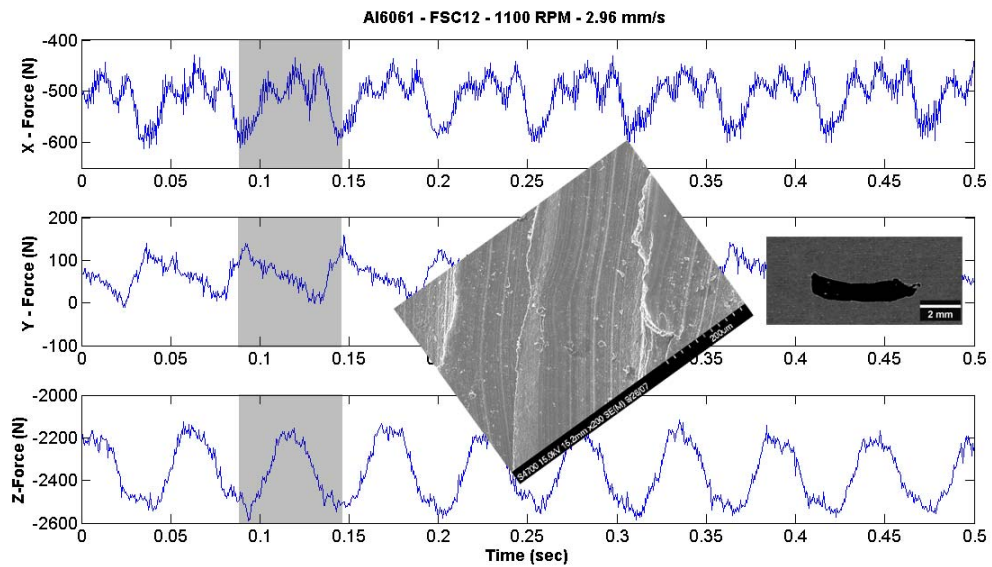


Figure 3.10 Force plots for 1100 rpm and 2.96 mm/sec using FSC12 with an inset of the channel. The SEM of the channel roof is overlaid. Shaded region shows the force profile for one complete rotation of the tool.

3.4. CONCLUSION

In this study, polar plots of the net resultant force acting on the pin during friction stir channeling were developed and analyzed to understand the relationship between the channel features and process parameters. It is shown that the position of the net force acting on the tool aids in predicting the occurrence of channels in the nugget. When channels exist in the nugget zone, the resultant force acting on the pin is in the region between the retreating side and the trailing edge. For nuggets with partial channels, the resultant force acts in the region between the trailing edge and the advancing side. The channels can be partially formed due to a combination of a lack of material flow from the base of the pin to the channel roof and the geometric features on the tool. Also, the magnitude of the forces reduces with an increase in the heat index of the process conditions.

A wider implication of the work done in this study is that this technique can be used for predicting the existence of voids in FSW/P nuggets. This technique can serve as an efficient non-destructive evaluation technique to study the FSW/P nuggets.

3.5. ACKNOWLEDGEMENT

The authors gratefully acknowledge the support of the National Science Foundation through grant CMMI-0523022 for this research.

3.6. REFERENCES

- [1] R. S. Mishra, Z. Y. Ma. Friction Stir Welding and Processing. Materials Science and Engineering R 2005, 50, 1-78.
- [2] R.S. Mishra in: R.S. Mishra, M. W. Mahoney (Eds.). Friction Stir Welding and Processing, ASM International, 2007; 309-350.
- [3] W. Arbegast. A Flow-Partitioned Deformation Zone Model for Defect Formation during Friction Stir Welding. Scripta Materialia, 2008. 58, 372-376.
- [4] R. S. Mishra. Integral Channels in Metal Components. US Patent 6,923,362, 2005.

- [5] N. Balasubramanian, R. S. Mishra, K. Krishnamurthy. Friction Stir Channeling: Characterization of the Channels. *Journal of Materials Processing Technology*, (manuscript submitted).
- [6] A.P. Reynolds. Flow Visualization and Simulation in FSW. *Scripta Materialia*, 2008. 58, 338-342.
- [7] H.N.B. Schmidt, T.L. Dickerson, J.H. Hattel. Material Flow in Butt Friction Stir Welds in AA2024-T3. *Acta Materialia*, 2006. 54, 1199–1209.
- [8] P. A. Colegrove, H. R. Shercliff. 3-Dimensional CFD Modelling of Flow Round a Threaded Friction Stir Welding Tool Profile. *Journal of Materials Processing Technology*, 2005. 169, 320-327.
- [9] P. A. Colegrove, H. R. Shercliff and R. Zettler. Model for Predicting Heat Generation and Temperature in Friction Stir Welding From the Material Properties. *Science and Technology of Welding and Joining*, 2007. 12(4), 284-297
- [10] D. G. Hattingh, T. I. van Niekerk, C. Blignault, G. Kruger, M. N. James. Analysis of the FSW Force Footprint and its Relationship with Process Parameters to Optimise Weld Performance and Tool Design. *Welding in the World*, 2004. 48 (1/2), 50-58
- [11] T. Long, A. P. Reynolds, Sci. Technol. Parametric studies of friction stir welding by commercial fluid dynamics simulation. *Science of Welding and Joining*, 2006. 11, 200-208.
- [12] J. H. Yan, M. A. Sutton, A. P. Reynolds. Processing and banding in AA2524 and AA2024 friction stir welding. *Science and Technology of Welding and Joining*, 2007. 12, 390-401.
- [13] W. Arbegast in: R.S. Mishra, M. W. Mahoney (Eds.). *Friction Stir Welding and Processing*. ASM International, 2007. 273-308.
- [14] C. Blignault, D. G. Hattingh, G. H. Kruger, T. I. van Niekerk, M. N. James. Friction stir weld process evaluation by multi-axial transducer. *Measurement*, 2008. 41, 32-43.
- [15] D. G. Hattingh, C. Blignault, T. I. van Niekerk, M. N. James. Characterization of the influences of FSW tool geometry on welding forces and weld tensile strength

using an instrumented tool. *Journal of Materials Processing Technology*, 2008. 203 46-57.

- [16] N. Balasubramanian, B. Gattu, R. S. Mishra. A Preliminary Study of the Process Forces during Friction Stir Processing of Aluminum Alloys. *Scripta Materialia*, (manuscript prepared).
- [17] W. Arbegast. Modeling friction stir joining as a metal working process. Hot deformation of aluminum alloys III, TMS, San Diego, CA, 2003. 313-327.
- [18] H Schmidt, J Hattel and J Wert. An Analytical Model for the Heat Generation in Friction Stir Welding. *Modelling and Simulation in Materials Science and Engineering*, 2004. 12, 143–157.

4. DEVELOPMENT OF A MECHANISTIC MODEL FOR FRICTION STIR CHANNELING

N. Balasubramanian¹, R. S. Mishra^{2,‡}, K. Krishnamurthy¹

¹ Department of Mechanical and Aerospace Engineering, Missouri University of Science and Technology, Rolla, MO 65409, USA

² Center for Friction Stir Processing, Department of Materials Science and Engineering, Missouri University of Science and Technology, Rolla, MO 65409, USA

ABSTRACT

A mechanistic model for the process specific energy as a function of the processing parameters during friction stir channeling (FSC) in Al 6061-T6 was developed and investigated. The thermal cycle acting on the surface of the workpiece was measured using an IR camera and the peak temperatures were studied as a function of the specific energy. The channel area is plotted against the process specific energy and analysed. A relationship between the processing conditions (tool rotational rate, traverse speed and plunge depth) and the channel area is defined.

Keywords: friction stir channeling, friction stir processing, specific energy, mechanistic model

4.1. INTRODUCTION

FSC is a non-traditional technique of creating continuous, integral channels in a monolithic plate in a single pass that is proposed as a method of manufacturing heat exchanging devices. FSC is based on the concept of converting wormhole defects that are formed during FSW into a continuous and stable channel. This technique relies on the frictional heat generated at the interface of the tool and the workpiece to soften and

[‡] Corresponding author. Tel.: +1-573-341-6361; e-mail: rsmishra@mst.edu

deform the material to create the channel. Mishra¹ has shown that by selecting the optimal processing parameters and reversing the material flow pattern of FSW, it is possible to achieve continuous channels. Balasubramanian et al.² have discussed about using the concept of FSC to create continuous channels along linear and curved profiles. There are two main aspects of FSC that differentiate it from FSW - (a) during FSC, a profiled tool is rotated in such a way that the material flows upwards towards the tool shoulder, and (b) an initial clearance is provided between the shoulder and the workpiece to deposit the material from the base of the pin.

During FSW/P, material flow and evolution of thermal cycle are considered to be the two most critical factors determining the properties of processed material. To predict the microstructural refinement and mechanical properties of the processed material, the thermal cycle acting on the workpiece has to be modelled. The thermal cycle during FSW/P depends on the heat generated at the tool-workpiece interface. The heat generation model should account for processing conditions, material properties and tool geometries. Various analytical, experimental and numerical methods have been utilized to model the generation and dissipation of heat during FSW/P. Thermal and mechanistic models have been developed based on Rosenthal's moving point-source equation³ to calculate the heat generation during FSW^{4,5}. Different analytical models for heat generation have been developed that account for tool geometry, contact conditions and energy input⁶⁻⁸. Frigaard et al.⁹ developed a numerical method based heat transfer model to determine the temperature distribution on a workpiece accounting for the interfacial pressure and geometry of tool. Arbogast developed a thermal model to define a relationship between the homologous temperature and process parameters¹⁰. Heurtier et al.¹¹ have predicted the heat generation on the basis of three sources namely, plastic strain, shoulder friction and pin friction.

In this study, a mechanistic model was developed to calculate the specific energy as a function of the process parameters. This specific energy is used to establish the relationship between process conditions and surface temperature and channel cross-sectional area. Experiments were conducted on Al6061-T6 to determine the model parameters and study the effectiveness of the model.

4.2. EXPERIMENTAL SET-UP

FSC runs were made on Al 6061-T6 plates of 6 mm thickness. The nominal composition of the plates was Al-1.0Mg-0.6Si-0.30Cu-0.20Cr. The tool used in this study had a shoulder diameter 16 mm with a cylindrical pin of 5 mm diameter and 4 mm height. The pin had left handed threads of 0.8 mm depth-of-cut and 75° angle running along its length. A total of nine runs were performed for this study. The list of processing parameters for the experiments is shown in Table 4.1.

Table 4.1 Processing parameters.

Plunge Depth (mm)	Tool Traverse Speed (mms^{-1})	Tool Rotation Rates (rpm)
3.0	1.69	1000, 1100, 1200
3.1	1.69	1000, 1100, 1200
3.2	1.69	1000, 1100, 1200

The experimental setup consisted of an IRB-940 Tricept 6-axis robot with three non-parallel telescopic translational joints and three rotational joints. The robot had a friction stir welding head from Friction Stir Link, Inc. The friction stir spindle assembly can rotate at rates up to 3000 rpm. The load rating of the spindle was 9 kN along the tool axis and 4.5 kN in the radial direction. During processing, the process forces and moments were logged at a frequency of 2000 Hz using a high frequency data acquisition system. Surface thermal measurements were made with the aid of a FLIR P-40 thermal camera. The surface temperature was measured at points at distances of 5, 10, 15, and 20 mm away from the circumference of the tool shoulder on either side of the traverse path. The thermal camera was placed at a distance of 300 mm away from the line of measurement and at an angle of 18° to the horizontal. A surface emissivity of 0.93 was input for the temperature measurement.

4.3. RESULTS AND DISCUSSION

4.3.1. Specific energy. The specific energy is defined as the ratio of power input to the process and traverse rate and is given by the equation

$$E = \frac{q}{v} \quad (1)$$

where q is the power input to the process and v is the traverse rate of the tool. The constitutive equation for power input is a function of the spindle torque and can be written as

$$q = \omega\tau \quad (2)$$

where ω is the tool rotation speed and τ is the spindle torque. The spindle torque increases with an increase in the resistance offered to the tool motion. It is dependent on the process parameters, namely, tool rotation speed, tool traverse rate, plunge depth and travel angle, and the surface area of contact between workpiece and tool. Torque has been observed to decrease with an increasing tool rotation rate and decreasing traverse speed. Also, an increase in the contact surface area of the tool with workpiece increases spindle torque. On the basis of these observations, spindle torque can be modelled as

$$\tau = A\omega^\alpha v^\beta d^\gamma \quad (3)$$

where A , α , β , and γ are constants to be determined using the method of least squares. As mentioned earlier, the value of torque (τ) decreases with increase in rotational speed (ω). This is due to the increase in the frictional heat generated at the tool-workpiece interface and the subsequent softening of the material. This requires α being negative, which would reduce the value of τ as ω increases. Also, the torque increases with an increase in the traverse rate due to a reduction in the preheating of material ahead of the tool and overall temperature. This requires β to be positive to increase τ . As the plunge depth increases, a

larger surface area of the tool is in contact with the workpiece and offers a larger resistance to the tool movement. This increases the value of the spindle torque, being represented by a positive value for γ . Substituting the expression obtained for spindle torque into equation (2) yields the expression for power input as

$$q = A\omega^{\alpha+1}v^{\beta}d^{\gamma} \quad (4)$$

The process specific energy is given by

$$E = \frac{q}{v} = A\omega^{\alpha+1}v^{\beta-1}d^{\gamma} \quad (5)$$

Using the method of least squares, the parameters and variables to be linearly related in equation (3) can be rewritten as

$$\ln \tau = \ln A + \alpha \ln \omega + \beta \ln v + \gamma \ln d \quad (6)$$

To solve for this equation, a set of nine experiments were done by varying the processing parameters. Table 4.2 shows the process parameters used to perform the set of nine experiments and the corresponding average values of the measured and modelled spindle torque. The values of the coefficient and indices obtained by using the method of least squares were $A = 3874.1$, $\alpha = -0.79$, $\beta = 0.11$, and $\gamma = 0.46$. The correlation coefficient was calculated to be 0.85 with a standard error of 0.42 Nm. From the coefficients and indices, it can be noted that the spindle torque increases with an increase in traverse rate, decrease in rotation speed and increase in plunge depth. The modelled coefficients are used to calculate input power to the system and the specific energy of the process. The table lists the value of the spindle power and the specific energy. It was seen that as the rotation speed increases, the input power increases due to an increased frictional heating effect. The same effect was seen with an increase in the plunge depth of the tool.

Table 4.2 List of process parameters with the measured and modelled torque, spindle power and specific energy.

Run No.	Plunge Depth (mm)	Rotational speed (rpm)	Traverse rate (mms^{-1})	Measured torque (Nm)	Modelled torque (Nm)	Spindle power (Js^{-1})	Specific energy, $\times 10^4$ (Jm^{-1})
1	3.0	1000	1.69	15.32	15.48	235.0	138800
2	3.0	1100	1.69	15.06	15.81	245.9	82980
3	3.0	1200	1.69	13.98	13.29	252.1	85090
4	3.1	1000	1.69	13.65	14.30	244.9	86700
5	3.1	1100	1.69	13.41	12.88	246.2	143060
6	3.1	1200	1.69	13.35	13.27	249.7	97000
7	3.2	1000	1.69	12.55	11.95	256.9	115720
8	3.2	1100	1.69	12.12	12.29	262.2	185170
9	3.2	1200	1.69	10.99	11.22	266.4	117980

4.3.2. Surface temperature profile. To determine the physical significance of the calculated specific energy, surface temperature was measured at different points on either side of the tool using the thermal camera for each of the run. The peak temperatures at each point on the plate were calculated from the measured thermal cycle. The thermal distribution along the workpiece surface is a function of the heat generated at the tool-workpiece interface and the thermal conductivity of the workpiece. The peak temperatures at the different points were measured and plotted as a function of pseudo heat index and specific energy, for every run. Figures 4.1(a) and 4.1(b) show the variation of the peak temperatures against heat index. The plot shows no distinct trend or relationship between the temperature and process parameters. The peak temperatures are then plotted against the calculated values of specific energy in Figures 4.2(a) and 4.2(b). From the figures, it is seen that there is a linear correlation between specific energy and peak temperature. The temperature increases with specific energy for all processing

conditions and for all points. An interesting trend is that the temperatures on the advancing side were greater than that of temperatures measured at the retreating side. The maximum temperature is at a point 5 mm away from the shoulder along the advancing side and was measured to be 182 °C. This temperature was measured for the processing parameter combination of 1100 rpm, 1.69 mms^{-1} at 3.2 mm plunge depth. Kalya et al.⁵ have reported peak temperatures of 220 °C close to the shoulder. This significant difference in the measured peak temperature can be attributed to reduction in frictional heat generated at the tool-workpiece interface. Unlike FSW, in FSC a clearance is provided between the tool and workpiece. The presence of this clearance between shoulder surface and workpiece decreases the contact area between the parent material and tool. In this study, the contact area between tool and workpiece was the maximum at a plunge depth of 3.2 mm. The peak temperature of 182 °C was measured for the process parameters at this plunge depth.

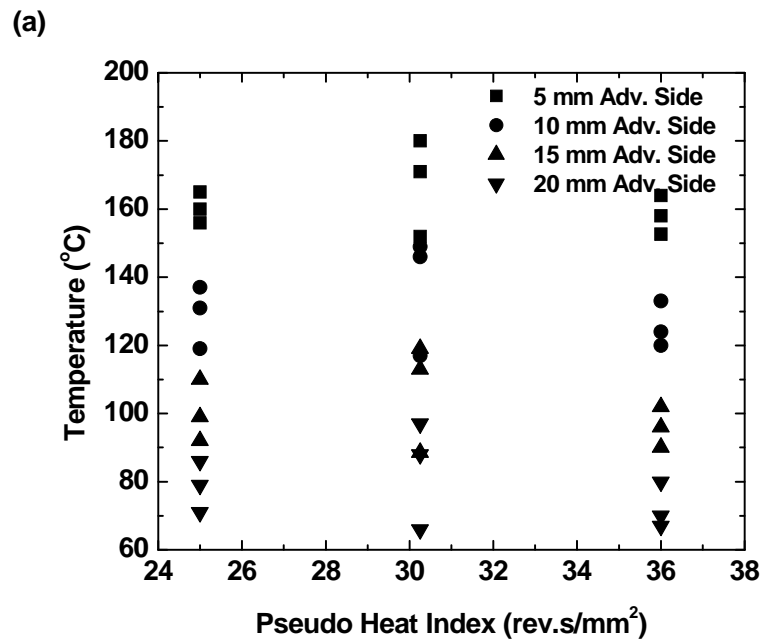


Figure 4.1 Variation of the peak temperatures against pseudo heat index along (a) advancing side, and (b) retreating side.

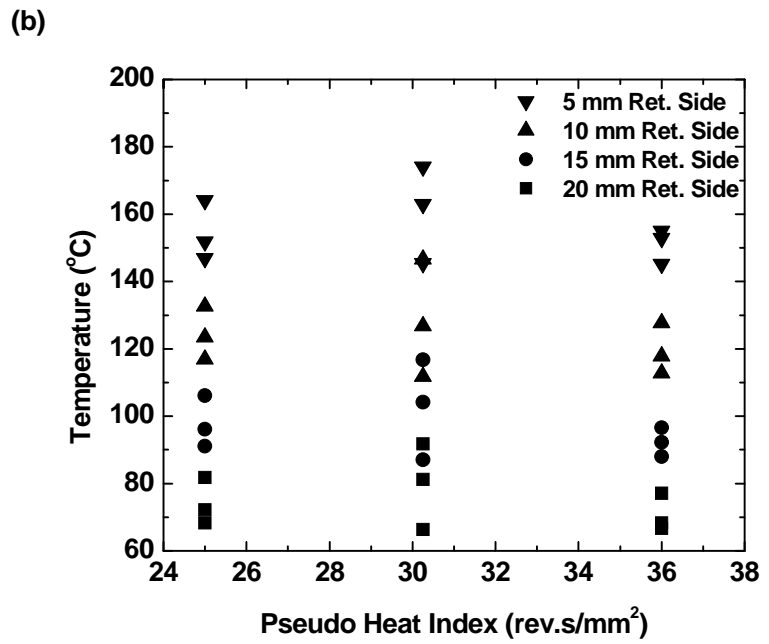


Figure 4.1 (Con't.) Variation of the peak temperatures against pseudo heat index along (a) advancing side, and (b) retreating side.

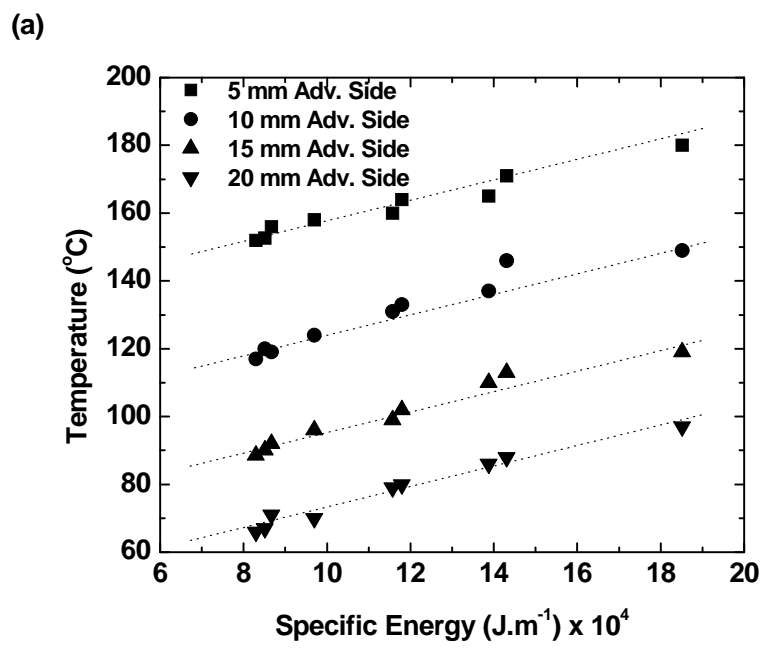


Figure 4.2 Variation of the peak temperatures against specific energy along (a) advancing side, and (b) retreating side.

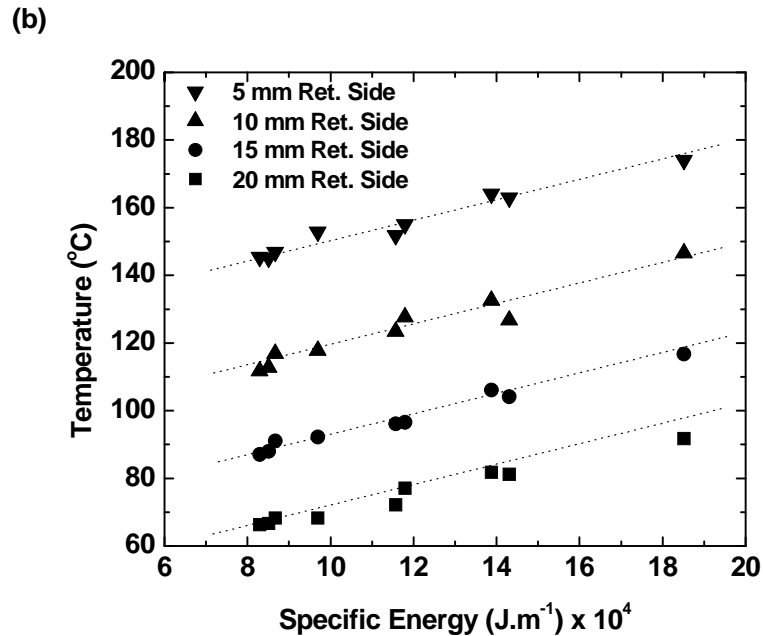


Figure 4.2 (Con't.) Variation of the peak temperatures against specific energy along (a) advancing side, and (b) retreating side.

4.3.3. Channel area. The processed material was sectioned, polished and observed under optical microscope. The channel cross-sectional area was measured from the macroscopic images. A plot of the variation of the channel area against heat index for different plunge depths is shown in Figure 4.3(a). From the figure it can be seen that the area is largest for the runs with the smallest plunge depth. The plot does not indicate any other trend between the channel area and the processing conditions. Figure 4.3(b) shows the relationship between channel area and process specific energy. A clear trend emerges for the variation of channel area with processing conditions. The channel area reduces with increasing specific energy. It can be inferred that with an increase in the tool rotation speed increases, the channel area decreases. An increase in the heat input to the process due to the high frictional heat results in the closure of the channels, thereby reducing its total area. Also, it is noticed that reducing the plunge depth increases the channel area. This is due to the fact that at lower plunge depths the clearance between shoulder and workpiece is larger and allows for a higher volumetric displacement of material from pin base.

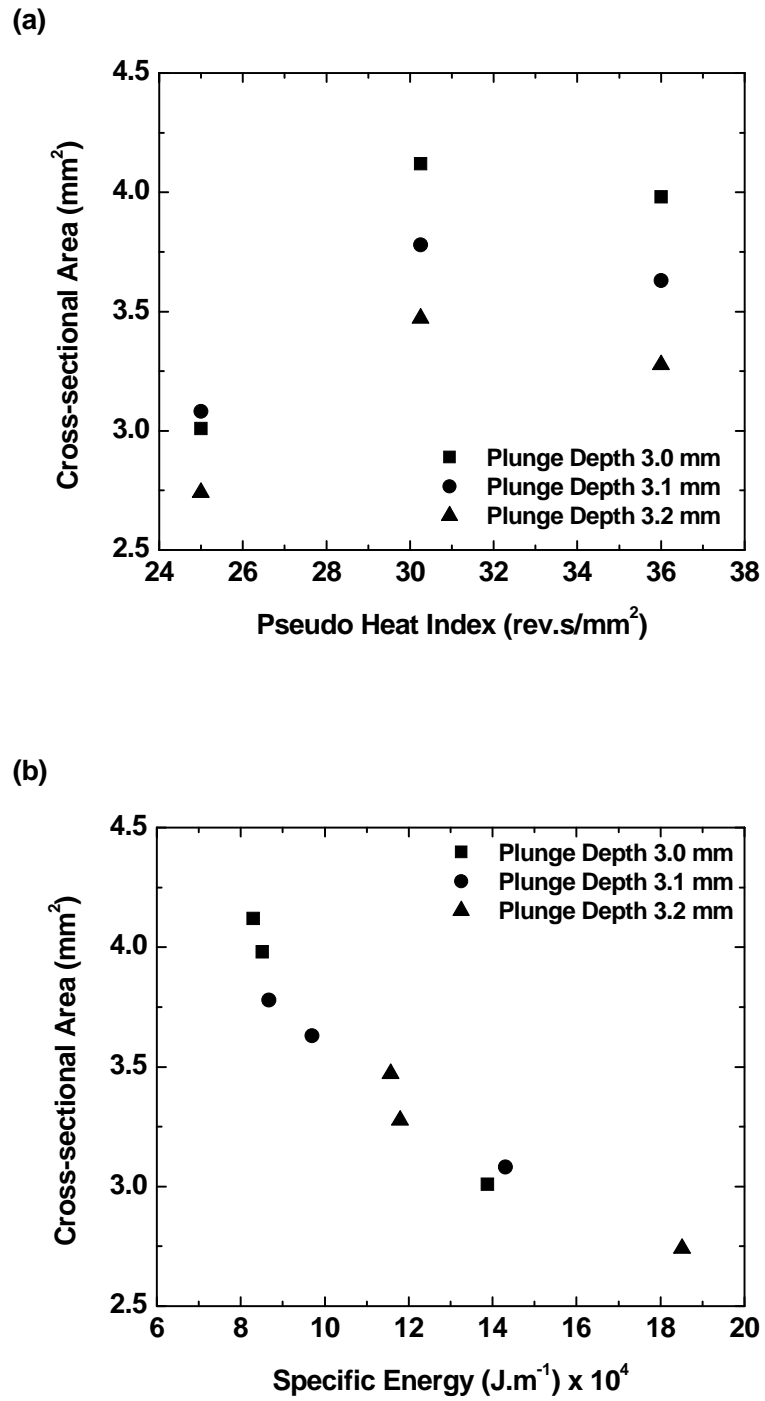


Figure 4.3 Variation of the channel area as a function of (a) pseudo heat index, and (b) specific energy.

4.4. CONCLUSIONS

Mechanistic models for the spindle torque and specific energy was developed as a function of tool rotation rate, traverse speed and plunge depth. The method of least squares technique was used to develop the model. The peak temperature of the FSC process shows a linear correlation against the specific energy of the process. As the specific energy increased, the peak temperature increases. The cross-sectional area decreases with increasing in specific energy.

4.5. ACKNOWLEDGEMENT

The authors gratefully acknowledge the support of the National Science Foundation through grant CMMI-0523022 for this research.

4.6. REFERENCES

- [1] R. S. Mishra: US Patent 6,923,362, 2005.
- [2] N. Balasubramanian, R. S. Mishra and K. Krishnamurthy: Journal of Materials Processing Technology, (manuscript submitted)
- [3] D. Rosenthal: Transactions of ASME, 1946, 68, 849-866.
- [4] J.C. McClure, W. Tang, L.E. Murr, X. Guo, Z. Feng, J.E. Gould: Proc. on 'Trends in Welding Research - American Welding Society / ASM International', Materials Park, OH, 1999, 590–595.
- [5] P. Kalya, K. Krishnamurthy, R. S. Mishra and J. A. Baumann: Proc. on 'Friction Stir Welding and Processing IV, TMS', Orlando, FL, 2007, 113-126.
- [6] H. Schmidt, J. Hattel and J. Wert: Modelling and Simulation in Materials Science and Engineering, 2004, 12, 143-157.
- [7] H. Schmidt and J. Hattel: Science and Technology of Welding and Joining, 2005, 10, 176-186.
- [8] M. Z. H. Khandkar, J. A. Khan and A. P. Reynolds: Science and Technology of Welding and Joining, 2003, 8, 165-174.

- [9] O. Frigaard, Ø. Grong and O. T. Midling: Proc. on 'Inalco '98: Seventh International Conference on Joints in Aluminium', Cambridge, UK, 1998, 208-218.
- [10] W. J. Arbegast: Proc. 3rd Symposium on 'Hot Deformation of Aluminum Alloys - TMS Annual Meeting', San Diego, CA, 2003, 313-327.
- [11] P. Heurtier, M.J. Jones, C. Desrayaud, J.H. Driver, F. Montheillet and D. Allehaux: Journal of Materials Processing Technology, 2006, 171, 348-357.

5. STUDY OF THE PRESSURE DROP AND HEAT TRANSFER THROUGH A FRICTION STIRRED CHANNEL

N. Balasubramanian¹, R. S. Mishra^{2,‡}, K. Krishnamurthy¹

¹ Department of Mechanical and Aerospace Engineering, Missouri University of Science and Technology, Rolla, MO 65409, USA

² Center for Friction Stir Processing, Department of Materials Science and Engineering, Missouri University of Science and Technology, Rolla, MO 65409, USA

ABSTRACT

Compact heat exchangers have certain unique features that make them efficient for numerous industrial applications. The efficiency of these heat exchangers is extremely high due to their light weight and high surface area density, which is greater than $700 \text{ m}^2/\text{m}^3$. Commercially available compact heat exchangers are currently fabricated in several steps by joining multiple tubes, or by independently fabricating and joining fluid channels. Friction stir channeling (FSC) is a simple and innovative technique of manufacturing heat exchangers in a single step in a monolithic material. In this paper, linear and curved channels with different hydraulic diameters are tested for pressure drop and heat transfer. The friction factor and the local heat transfer coefficient of the channels area calculated. The thermal behavior of a friction stirred channel is simulated using the commercial CFD package FLUENT.

Keywords: friction stir channeling, minichannels, compact heat exchangers, surface roughness, friction factor

5.1. INTRODUCTION

Due to their efficient performance, compact heat exchangers are being increasingly employed in many process applications in the automotive, aerospace,

[‡] Corresponding author. Tel.: +1-573-341-6361; e-mail: rsmishra@mst.edu

microelectronics and biomedical industries. Their higher pumping power requirements are compensated by the overall size of the heat exchangers and cost reductions. These heat exchangers have a surface area density higher than $700 \text{ m}^2/\text{m}^3$, i.e., they have a higher heat transfer surface area per unit volume [1]. These heat exchangers have fluid flow passages that vary from a few millimeters to microns. Fluid flow in the minichannels has emerged as an important area of research, motivated by their use in diverse applications as micropower generation, , computer chips, chemical separations processes, vehicular heat exchangers, condensers and evaporators in air-conditions and refrigeration industry, aircraft oil-coolers, automotive radiators, intercoolers or compressors and other applications that require small volume and light weight.

Heat exchangers are currently manufactured in multiple steps by joining multiple tubes using conventional metal fabricating and joining techniques. Wadekar [2] has discussed the current manufacturing techniques used for different commercial heat exchangers. Conventional shell and tube heat exchangers are made from 8 mm to 60 mm diameter tubes that are joined using welding and other metal joining processes. The plate heat exchangers have a hydraulic diameter of 5 to 6 mm and are also joined using welding, brazing, and other conventional techniques. Tube-fin and Plate-fin heat exchangers (for example, car radiators) have a typical diameter of 2 to 3 mm, and are fabricated using brazing. Printed circuit heat exchangers (PCHE) have channels with hydraulic diameters of 1 to 2 mm. Diffusion bonding and brazing techniques are used for PCHEs. Compact heat exchangers with micro- and meso-scale channels are generally manufactured using techniques like chemical etching, micro-fabrication, precision machining, and selective laser melting [3, 4].

FSC is a non-traditional technique of creating continuous, integral channels in a monolithic plate in a single pass. It is an off-shoot of friction stir processing (FSP) and it is proposed as a method of manufacturing compact mini-channel heat exchanging devices. FSP is an adaptation of friction stir welding (FSW) that builds upon some of the unique features of FSW like the extensive plastic flow of material, the low amount of heat generated, and the absence of flaws and pores to develop new processes [5]. In FSW, a non-consumable tool is rotated under an imposed normal load and then plunged into the workpiece. A frictional and deformational heat is generated between the tool and work

material that causes the plastic deformation of the material at an elevated temperature, resulting in a fine-grained microstructure in the stirred region (called a “nugget”) [6-8]. During FSW a defect referred to as a “wormhole” is generated if the processing parameters are not optimal. Arbegast [9] has discussed the formation of different defects during FSW, including wormhole generation. The occurrence of wormholes in the FSW nugget has been attributed to flow defects because of the non-optimal processing conditions or geometry of the tool features. FSC is established on the theory of converting this defect formation into a continuous and stable channel. Mishra [10] has achieved a continuous hole in a single plate by selecting the optimal processing parameters and reversing the material flow pattern of FSW. N. Balasubramanian et al. [11] have discussed about using the concept of FSC to create continuous channels inside monolithic plates. The channel formation process has been dealt in detail and the channel has been characterized for its size, shape and internal features. The technique also examines the continuity of the channels long linear and curved profiles.

In any heat exchange appliance, the most important characteristic dimension of a channel is its hydraulic diameter D_h . The hydraulic diameter is a term commonly used when handling flow in noncircular tubes and channels. It is defined as the ratio of four times the area of the cross-section to the wetted perimeter of the channel. On the basis of the hydraulic diameter, compact heat exchangers have been classified into micro-heat exchangers ($D_h = 1 - 100$ microns), meso-heat exchangers ($D_h = 0.0001 - 1$ mm), compact heat exchangers ($D_h = 1 - 6$ mm) and conventional heat exchangers ($D_h > 6$ mm) [12]. A different system of classification on the basis of minimum channel dimension has been proposed by Kandlikar [13, 14] and is shown in Table 5.1. The channels obtained using FSC have a D_h ranging from 0.2 mm to 2 mm and can be categorized as mini-channels on the basis of Kandlikars’ classification.

Table 5.1 Channel Classification [14]

Conventional channels	$D > 3 \text{ mm}$
Mini-channels	$3 \text{ mm} \geq D > 200 \text{ }\mu\text{m}$
Micro-channels	$200 \text{ }\mu\text{m} \geq D > 10 \text{ }\mu\text{m}$
Transitional channels	$10 \text{ }\mu\text{m} \geq D > 0.1 \text{ }\mu\text{m}$
Transitional micro-channels	$10 \text{ }\mu\text{m} \geq D > 1 \text{ }\mu\text{m}$
Transitional nano-channels	$1 \text{ }\mu\text{m} \geq D > 0.1 \text{ }\mu\text{m}$
Molecular nano-channels	$0.1 \text{ }\mu\text{m} > D$

In this paper, channels with varying hydraulic diameters and roughness heights are tested for their pressure drop. The heat transfer coefficient and the friction factor are calculated and analyzed. The pressure drop for channels along curves is measured and the values are compared with simulations.

5.2. EXPERIMENTAL SET-UP

Commercial 6061 Al alloy was selected for the fabrication of these channels. The friction stir tools used in the study were made of MP-159 (Ni-Co superalloy) and the intent of these runs was to fabricate channels with no surface defects but with maximum size. The process parameters (the tool rotation rate, traverse speed, and the plunge depth) were varied to obtain the channels. Optical microscopy was used to measure and characterize the size and shape of the channels.

Six channels along straight lines were fabricated using FSC, each to a length of 120 mm. Three channels that had a U- profile were created to study for the performance along curves. The channels were created at a depth of 3.1 mm in a plate of 6.3 mm thickness. Table 5.2 lists the set of experimental parameters that were investigated for this study. The hydraulic diameters with an asterisk (*) next to it denote the channels that were created along curved profiles. The hydraulic diameter, area and the roughness height on the inside walls of the channels were measured by taking a cross-section and studying under an optical microscope.

Table 5.2 Range of experimental parameters investigated. All tests were conducted with the water as the test fluid

Hydraulic diameter of channel, D_h (mm)	Roughness height of channel, ε (mm)	Area of channel (mm^2)	ε/D_h	Reynolds number, Re
0.84	0.042	2.71	0.0504	570-2850
0.89*	0.042	2.131	0.04757	524-2619
0.98	0.084	2.97	0.08639	549-2750
1.06*	0.084	3.26	0.07987	541-2710
1.25	0.084	3.763	0.06784	552-2764
1.38*	0.127	4.14	0.09203	555-2778

An experimental set-up was developed for measuring the pressure drop and temperature difference between inlet and outlet. The schematic of the set-up is shown in Figure 5.1. The test fluid used in the study was water, stored in a glass container and heated using a heat plate to 45°C. It was pumped from the container using a miniature gear pump. A needle valve was used to regulate the flow rate of water into the test section and a flow meter was used to determine the flow rate of the fluid passing through the tubes. A pressure transducer measured the differential pressure of water entering and exiting the test channels. Thermocouples were inserted at the inlet and outlet of the channels to measure the temperature. The pressure transducer and the thermocouple readings were data logged using an NI data acquisition card. The tubes and the fittings were covered with insulating tapes to prevent any loss of heat to the surrounding environment. The bottom surface of the test sections was insulated to prevent heat loss to the base table. The other surfaces of the workpiece were assumed to transfer heat to the surrounding environment through natural convection.

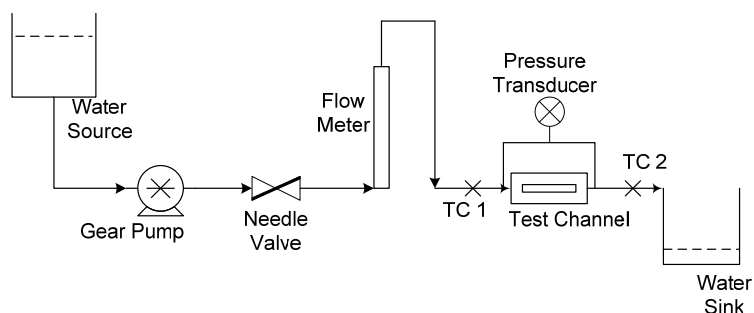


Figure 5.1 A schematic of the experimental setup.

5.3. RESULTS AND DISCUSSION

The shapes of the channels obtained from FSC technique do not resemble any well-defined standard geometry like a circle or a rectangle. Balasubramanian et al. [11] have discussed about the variation of the channel shapes with the process input parameters during FSC. Figure 5.2 shows the variation of the shape of the channel with regard to the process parameters. Figure 5.3 shows the longitudinal cross-section of a channel obtained using FSC.

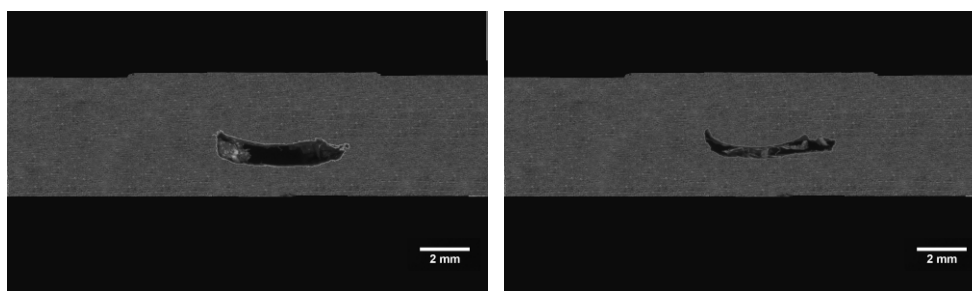


Figure 5.2 Cross-section of the channels depicting the variation of channel shapes with processing parameters. (a) 1100 rpm, 2.96 mm/sec and (b) 1200 rpm, 2.11 mm/sec.

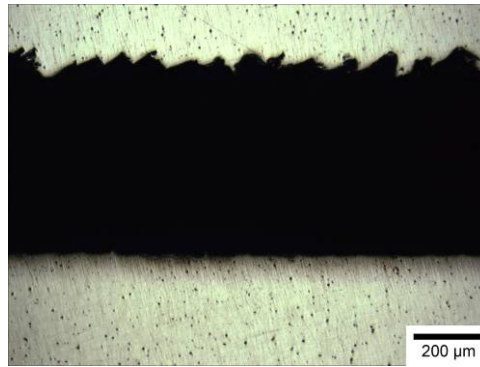


Figure 5.3 Longitudinal cross-section of the channel showing the roughness on the roof of the channels (1200 rpm, 2.11 mm/sec).

It can be noted that the features of the channels walls vary at the lower and upper surfaces of the channels. The bottom of the channel is relatively smooth and flat and the top surface of the channel was rough and undulated. The surface roughness at the upper surface of the channel was uniformly spaced. The periodicity of the roughness at the top surface was measured and it matched with the amount of material that was displaced with each rotation of the tool (the rate of tool advance per rotation). The hydraulic diameters of these channels ranged from 0.8 mm to 1.4 mm and the roughness height varied from 0.04 mm to 0.127 mm. The experiments were done for five different flow rates and the pressure drop and temperature difference were measured and plotted against the flow rate.

Figure 5.4 shows the pressure drop measured across the channels as a function of the mass flow rate for different channel diameters. The pressure drop inside the channels was in the range of 4500 – 7000 Pa. The Reynolds number, Re varied from 500 to 2850 for the combination of flow rates and hydraulic diameters. The flow was in the laminar and laminar-turbulent transition zones.

It can be noted that channels with the smallest hydraulic diameter exhibit the largest pressure drop across the test section. As the channel hydraulic diameter and the cross-sectional area increases, the pressure drop decreases. The pressure drop across the channels is due to the presence of roughness features on the interior surface and also the

irregular shape of the channel. The surface roughness along the fluid flow path encourages localized pressure drop. Also, the flow transitions into the turbulent flow regime when surface undulations exist. The dependence of the laminar-to-turbulent transition on the relative roughness features along flow path has been investigated and reported in the literature [15, 16].

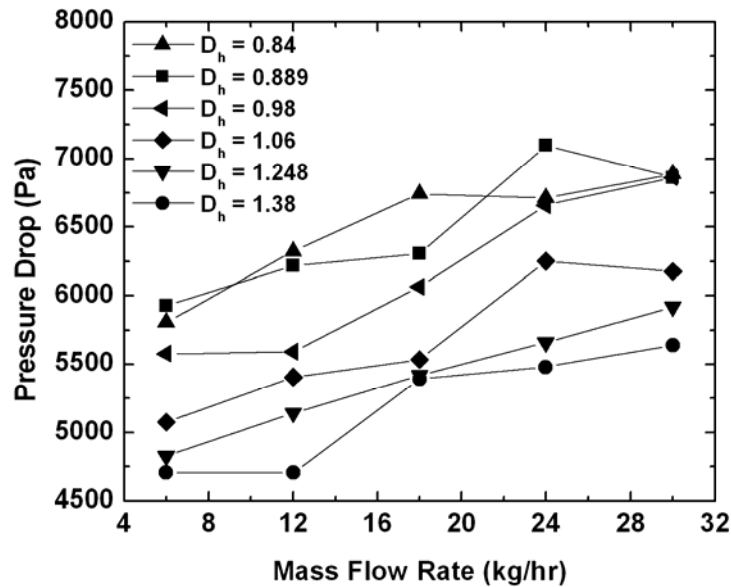


Figure 5.4 Measured pressure drop for channels with different hydraulic diameters.

Moody's diagram is a representation of the friction factor of flow surfaces over a wide range of Reynolds numbers and relative roughness values ranging between 0 and 0.05. The friction factor is a dimensionless number used in fluid flow calculations. It is the ratio of the shear stress at the wall to the flow kinetic energy per unit volume. It is given by the relation:

$$f = \frac{\Delta p}{4 \left(\frac{L}{D} \right) \rho \frac{V^2}{2}} \quad (1)$$

where f depends on the Reynolds number and the roughness of the pipe surface. Moody's chart serves as an easy way to estimate the friction factor across channels without doing experiments. The chart shows that in a fully developed laminar flow, f is independent of relative roughness, ε/D_h . Figure 5.5 shows the friction factor (f), versus the Reynolds number (Re), for different ε/D_h values of the friction stirred channels. The ε/D_h values vary from 0.05 to 0.092 and the friction factor is calculated using the Equation 1.

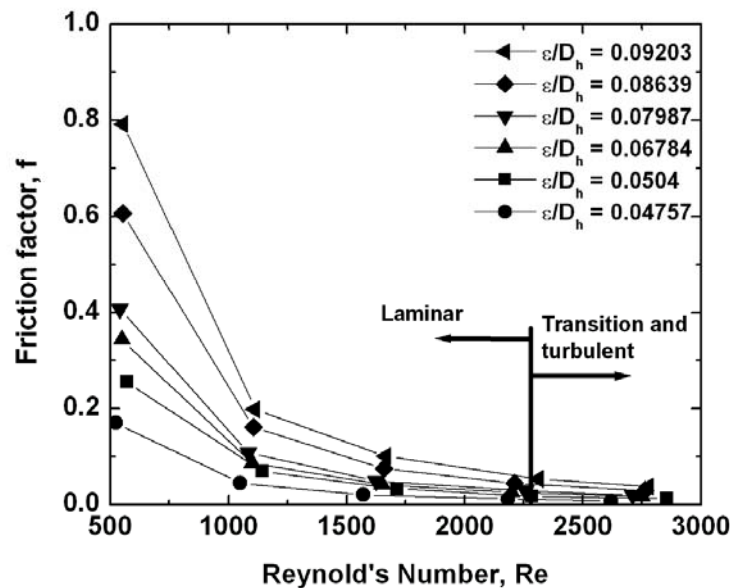


Figure 5.5 Plot of the calculated heat transfer coefficient for the different channels at different flow rates.

The pressure drops along these channels increased with increasing flow rates and the resulting friction factor decrease with increasing flow rates. The figure shows that the channels with the lowest ε/D_h exhibited lower friction factors than the larger channels. The roughness inside the channels had a more pronounced effect on the friction factor. The value of f decreases with a decrease in relative roughness. This trend follows the behavior that has been shown in Moody's chart. This chart when further developed to include more relative roughness values will be helpful in predicting the pressure drop across the channels.

Figure 5.6 shows the variation of the local heat transfer coefficient, h , against mass flow rate. It can be seen that the heat transfer coefficient increases with an increase in the mass flow rate. Heat transfer coefficient increases with reducing hydraulic diameter. The heat transfer coefficients increase as the flow was into the forced convection regime and turbulent flow.

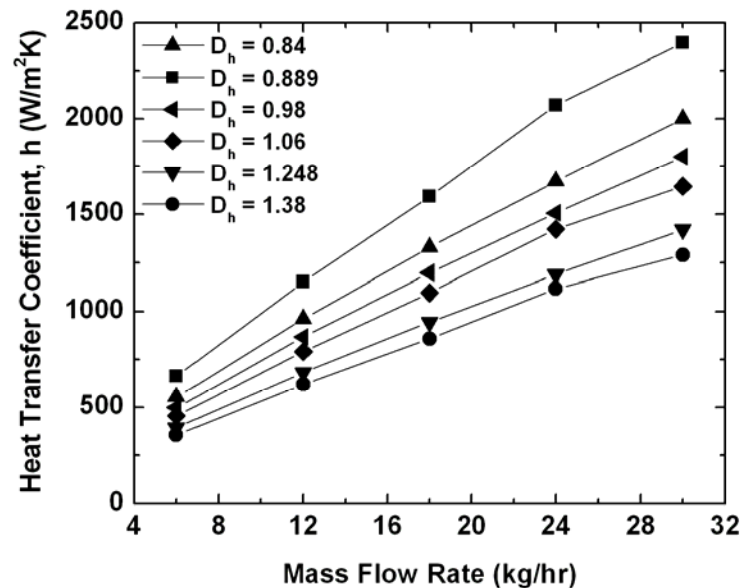


Figure 5.6 Measured heat transfer coefficient of the channels.

Figure 5.7 shows the pressure drop measured across the channels along curved profile as a function of the mass flow rate. The pressure drop inside these channels varied from 12000– 35000 Pa. The Reynolds number, Re of the test conditions vary from 520 to 2780 for different flow rates and hydraulic diameters. It can be noted that the pressure drop across these channels was extremely high when compared to channels along straight lines. An increase in the pressure drop along curves was along the expected lines but the magnitude of variation in comparison to the straight channels was extremely high for the testing conditions. This is due to the effect of the small constriction in the channel size along the curves during the fabrication process [11]. Also the non-linearity of the channel shape is a contributing factor to the high variation.

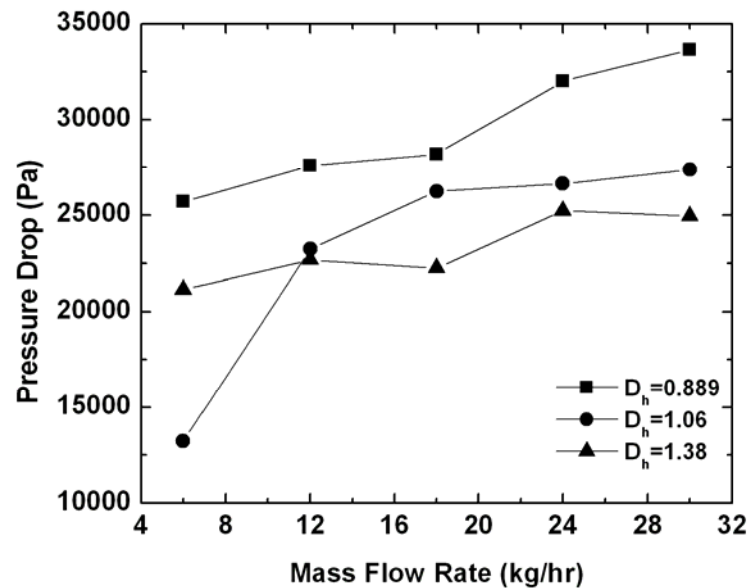


Figure 5.7 Measured pressure drop across the channels along curves.

A simulation to calculate the pressure drop along the channel length was done using the commercial CFD package, FLUENT. The test channel was modeled and meshed using GAMBIT. The dimension of the rectangular block with a channel inside it was 120 mm x 80 mm x 6.35 mm. The channel shape was assumed to be a trapezium and the cross-sectional area and the hydraulic diameters were modeled to be closer to the actual test sections. A simple but refined mesh with 170000 hexahedral elements was created. Coupled heat transfer boundary condition was given at the channel walls where it interacts with the fluid and convective boundary conditions were given to the outside surfaces of the rectangular block. Turbulent flow condition was used to provide the roughness height in the inside walls of the channels. The roughness heights input in the study were the actual values measured for each of the test channels. For the simulation, the heat transfer coefficient of the fluid was input from the experimentally derived values shown in Figure 5.5. The results of pressure drop across the channel are plotted against the mass flow rate and shown in Figure 5.8. The simulation results show an increase in the pressure drop with a decrease of the channel size. Also, the differential pressure is

high at higher flow rates. Figure 5.9 shows the simulated pressure drop across channels along curved profiles.

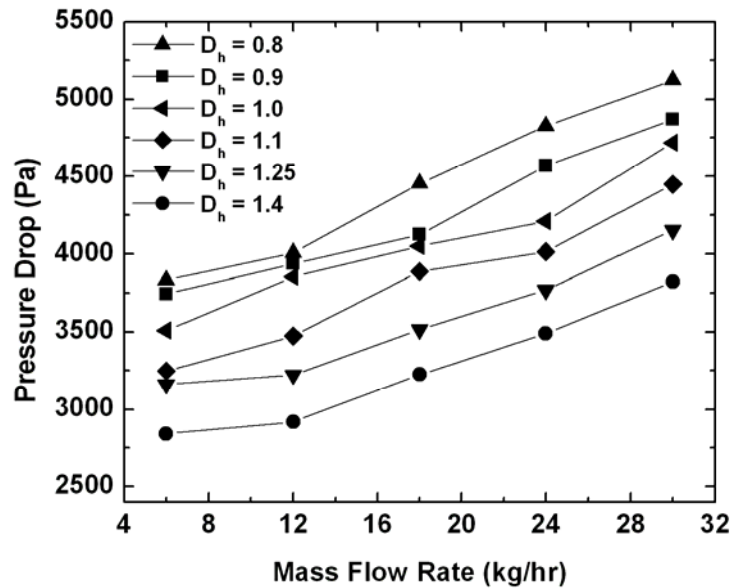


Figure 5.8 Simulated pressure drop along linear channels with different hydraulic diameters.

From Figure 5.8 and Figure 5.9, it can be seen that the magnitude of pressure drop across channels along curves was much higher. But the simulated values for both the cases were much lower in comparison to the measured values. One reason for the high pressure drop in the measured values was the non-linearity of the channel shapes and the difficulty in modeling the same. Also the roughness patterns in the simulation are assumed to be equally spaced and uniform in their dimensions, while in the test channels there will be an inherent variation in the dimensions due to the non-linearities associated with the machining process.

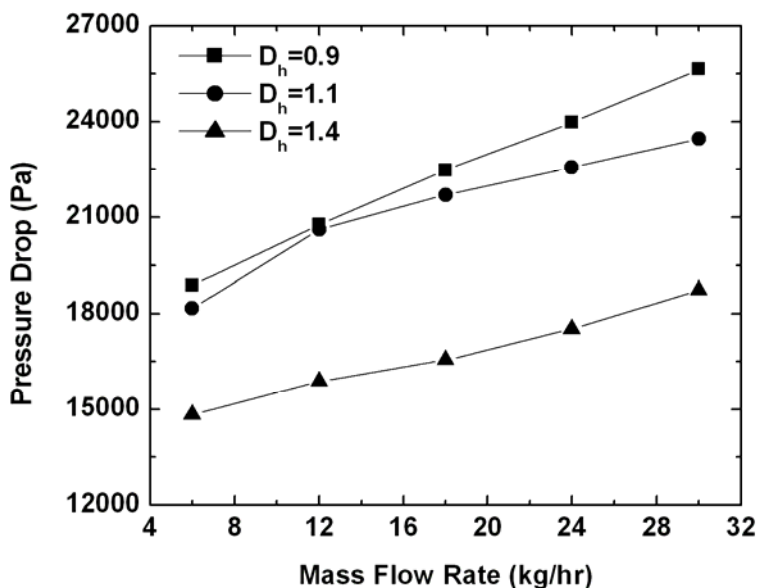


Figure 5.9 Simulated pressure drop across channels along curves and with different hydraulic diameters.

5.4. CONCLUSION

In summary, minichannels with hydraulic diameters varying from 0.8 mm to 1.4 mm were fabricated using FSC technique and their performance was evaluated. A test fluid (water) was passed through a set of these channels to measure the drop in pressure and the change in the inlet and outlet temperatures. The friction factors of the channels with different relative roughness were calculated and a friction chart was developed. It showed that channels with smaller relative roughness have lower friction factors and it decreased with increasing flow rates. The pressure drop across the channels increased with decreasing channel sizes and at higher flow rates. This was true for channels along linear and curved profiles. CFD simulations for similar flow indicated the same trend.

5.5. ACKNOWLEDGMENTS

The authors wish to acknowledge the support of the National Science Foundation through grant DMI-0523022 for this research.

5.6. REFERENCES

- [1] T. Kuppan, "Heat Exchanger Design Handbook," CRC, 1st edition, 2000.
- [2] V.V. Wadekar, "Heat Exchangers in Process Industry and Mini- and Microscale Heat Transfer," Proceedings of Fifth International Conference on Enhanced, Compact and Ultra-Compact Heat Exchangers: Science, Engineering and Technology, 2005, pp. 318.
- [3] S. Tsopanos, C. J. Sutcliffe, I. Owen, "The Manufacture of Micro Cross-Flow Heat Exchangers by Selective Laser Melting," Proceedings of Fifth International Conference on Enhanced, Compact and Ultra-Compact Heat Exchangers: Science, Engineering and Technology, 2005, pp. 410-417.
- [4] M. Christophe, W. K. Kevin, "Fabrication and Performance of a Pin Fin Micro Heat Exchanger," Journal of Heat Transfer, vol. 126, pp. 434 – 444, 2004.
- [5] W.M. Thomas, E.D. Nicholas, J.C. Needham, M.G. Murch, P. Templesmith, C.J. Dawes, G. B. Patent Application No, 9125978.8 (1991).
- [6] K. Colligan, "Relationships between Process Variables Related to Heat Generation in Friction Stir Welding of Aluminum," Friction Stir Welding and Processing IV, TMS Annual Meeting, Orlando, Fl, pp. 39-52, 2007.
- [7] H. R. Shercliff, P. A. Colegrove, "Modelling of friction stir welding", Mathematical Modelling of Weld Phenomena 6, eds. H. Cerjak and H. Bhadeshia, Maney Publishing, London, UK, pp. 927-974, 2002.
- [8] R. S. Mishra, "Preface to the Viewpoint Set on friction stir processing", Scripta Materialia v 58, n 5, pp 325-326, 2008.
- [9] W. Arbegast, "A Flow-Partitioned Deformation Zone Model for Defect Formation during Friction Stir Welding," Scripta Materialia, 58, pp.372-376, 2008.
- [10] R. S. Mishra. Integral Channels in Metal Components. US Patent 6,923,362, 2005.
- [11] N. Balasubramanian, R. S. Mishra, K. Krishnamurthy, "Friction Stir Channeling: Characterization of the Channels," Journal of Materials Processing Technology, (manuscript submitted).

- [12] S. S. Mehendale, A.M. Jacobi, R.K. Shah, "Fluid Flow and Heat Transfer at Micro- and Meso-Scales with Application to Heat Exchanger Design," *Applied Mechanical Review*, 53, 2000, pp. 175-193.
- [13] S.G. Kandlikar, W.J. Grande, "Evolution of Microchannel Flow Passages - Thermohydraulic Performance and Fabrication Technology," *Heat Transfer Engineering*, 24, 2003, pp. 3-17.
- [14] S. G. Kandlikar, "A roadmap for implementing minichannels in refrigeration and air-conditioning systems - Current status and future directions," *Heat Transfer Engineering*, v 28, n 12, pp. 973-985, 2007.
- [15] G. M. Mala, D. Li, "Flow characteristics in microtubes," *International Journal Heat and Fluid Flow* 20, pp.142-148, 1999.
- [16] B. X. Wang, X. F. Peng, "Experimental investigation on liquid forced convection heat transfer for liquid flowing through microchannel," *International Journal of Heat and Mass Transfer*, 30, pp.73-84, 1994.

6. CONCLUSIONS AND SCOPE OF FUTURE WORK

The research work for this dissertation developed friction stir channeling (FSC) as a manufacturing process for creating channels that can be used in heat exchanging equipments. It was shown during the course of this study that FSC can create stable internal channels in monolithic plates. The channels were continuous along linear and curved profiles. The variation of the channel features with processing parameters for a given set of tool geometries was studied and process maps were. The science behind the formation of the channels during FSC was explained by analyzing the process forces during FSC and it has been proposed that polar plots of the net resultant forces can predict the existence of channels in the FSC nugget. While the science of FSW/P is still evolving, the current study was able to answer some questions on the formation of voids during FSP. This work can be extended by employing process force analysis as a non-destructive evaluation technique for predicting the existence of voids in FSW/P nuggets. It was established that the specific energy of the process is a good indicator of the variation of the channel size. The scope of this work can be widened to correlate the characteristics of FSW/P nuggets with the processing parameters.

The performance of the channels created using FSC was studied by experimentally determining the pressure drop across the channels. The friction factor and heat transfer coefficient of the channels was calculated and studied as a function of the relative roughness of the channels. While it is apparent from the results that pressure drop across the channels can be reduced by increasing the cross-sectional area of the channels, further work needs to be done to understand the influence of channel roughness and irregular shape of channels on the performance, especially in a heat exchanger assembly. Also, the wearing of the surface roughness with time and its effect on the channel performance needs to be studied. The fouling and corrosion characteristics of the channels can also be studied to evaluate the feasibility of using these channels in commercial applications.

7. BIBLIOGRAPHY

- [1] W. M. Thomas, E. D. Nicholas, J. C. Needham, M. G. Murch, P. Templesmith, and C. J. Dawes, "Friction Stir Butt Welding," G. B. Patent No. 9125978.8, International Patent No. PCT/GB92/02203, 1991.
- [2] B. London, M. Mahoney, W. Bingel, M. Calabrese, and D. Waldron, "Experimental Methods for Determining Material Flow in Friction Stir Welds," Third International Symposium on Friction Stir Welding, Kobe, Japan, 2001.
- [3] J. H. Record, J. L. Covington, T. W. Nelson, C. D. Sorensen, B. W. Webb, "A look at the statistical identification of critical process parameters in friction stir welding", *Welding Journal*, v 86, n 4, pp 97-s-103-s, 2007.
- [4] Johnson, R., 2001, "Forces in Friction Stir Welding of Aluminum Alloys," Third International Symposium on Friction Stir Welding, Kobe, Japan.
- [5] R. S. Mishra, Z. Y. Ma, "Friction Stir Welding and Processing," *Materials Science and Engineering R*, v 50, pp 1-78, 2005.
- [6] W. Arbegast, "Application of Friction Stir Welding and Related Technologies," *Friction Stir Welding and Processing*, ASM International, 1st edition, eds. R.S. Mishra, M. W. Mahoney, Chapter 13, pp 273-308, 2007.
- [7] R. S. Mishra, "Integral channels in metal components," US Patent 6,923,362, 2005.
- [8] K. Colligan, "Relationships between Process Variables Related to Heat Generation in Friction Stir Welding of Aluminum," *Friction Stir Welding and Processing IV*, TMS Annual Meeting, Orlando, Fl, pp. 39-52, 2007.
- [9] H. R. Shercliff, P. A. Colegrove, "Modelling of friction stir welding", *Mathematical Modelling of Weld Phenomena 6*, eds. H. Cerjak and H. Bhadeshia, Maney Publishing, London, UK, pp. 927-974, 2002.
- [10] R. S. Mishra, "Preface to the Viewpoint Set on friction stir processing", *Scripta Materialia* v 58, n 5, pp 325-326, 2008,.
- [11] R.K. Shah, D. P. Sekulic, "Fundamentals of Heat Exchanger Design," Wiley, 2003.
- [12] T. Kuppan, "Heat Exchanger Design Handbook," CRC 1st edition, 2000.

- [13] T. A. Trabold, "Minichannels in Polymer Electrolyte Membrane Fuel Cells," *Heat Transfer Engineering*, vol. 26, pp. 3-12, 2005.
- [14] S. Kakac, H. Liu, "Heat Exchangers: Selection, Rating and Thermal Design," CRC Press, 2002.
- [15] W. M. Kays, A. L. London, "Compact Heat Exchangers," Krieger Publishing Company; 3rd edition, 1998.
- [16] S. S. Mehendale, A.M. Jacobi, R.K. Shah, "Fluid Flow and Heat Transfer at Micro- and Meso-Scales with Application to Heat Exchanger Design," *Applied Mechanics Review*, 53, pp. 175-193, 2000.
- [17] S.G. Kandlikar, W.J. Grande, "Evolution of Microchannel Flow Passages - Thermohydraulic Performance and Fabrication Technology," *Heat Transfer Engineering*, 24, pp. 3-17, 2003.
- [18] A. Kawahara, M. Sadatomi, K. Okayama, M. Kawaji, and P. M.-Y. Chung, "Effects of Channel Diameter and Liquid Properties on Void Fraction in Adiabatic Two-Phase Flow through Microchannels," *Heat Transfer Engineering*, v 26, n 3, pp. 13–19, 2005.
- [19] V. V. Wadekar, "Heat Exchangers in Process Industry and Mini- and Microscale Heat Transfer," *Proceedings of Fifth International Conference on Enhanced, Compact and Ultra-Compact Heat Exchangers: Science, Engineering and Technology*, pp. 318 – 325, 2005.
- [20] S. Tsoupanos, C. J. Sutcliffe, I. Owen, "The Manufacture of Micro Cross-Flow Heat Exchangers by Selective Laser Melting," *Proceedings of Fifth International Conference on Enhanced, Compact and Ultra-Compact Heat Exchangers: Science, Engineering and Technology*, 410-417, 2005.
- [21] M. Christophe, W. K. Kevin, "Fabrication and Performance of a Pin Fin Micro Heat Exchanger," *Journal of Heat Transfer*, vol. 126, pp. 434 – 444, 2004.
- [22] J.J. Brandner , E. Anurjew, L. Bohn, E. Hansjosten, T. Henning, U. Schygulla, A. Wenka, K. Schubert, "Concepts and Realization of Microstructure Heat Exchangers for Enhanced Heat Transfer," *Experimental Thermal and Fluid Science*, 30, pp. 801-809, 2006.

- [23] T.M. Adams, S.I. Abdel-Khalik, S.M. Jeter, Z.H. Qureshi, "An experimental investigation of single-phase forced convection in microchannels," *International Journal of Heat Mass Transfer*, v 41, pp. 851–857, 1998.
- [24] X.F. Peng, G.P. Peterson, "Convective heat transfer and flow friction for water flow in microchannel structures," *International Journal of Heat Mass Transfer*, v 39, pp. 2599–2608, 1996.
- [25] H. Darcy, *Recherches Experimentales Relatives au Mouvement de L'Eaudans les Tuyaux*, Mallet-Bachelier, Paris, France, 1857.
- [26] J. T. Fanning, *A Practical Treatise on Hydraulic and Water Supply Engineering*, Van Nostrand, New York, 1877; revised ed. 1886.
- [27] J. Nikuradse, "Laws of flow in rough pipes" English translation of NACA Technical Memorandum 1292, 1937.
- [28] S.G. Kandlikar, D. Schmitt, A.L. Carranoc, J.B. Taylor, "Characterization of surface roughness effects on pressure drop in single-phase flow in minichannels," *Physics of Fluids*, v 17, pp. 100606-1 - 100606-11, 2005.
- [29] J. H. Wang, H. Y. Yeh, R. J. Shyu, "Thermal-Hydraulic Characteristic of Micro Heat Exchangers," *Mechanical Sensors, Actuators and Systems*, ASME 32, pp. 331–339, 1991.
- [30] D. Westphalen, K. W. Roth, J. Brodrick, "Microchannel Heat Exchangers," *ASHRAE Journal*, v 45, n 12, pp. 107–109, 2003.
- [31] S. G. Kandlikar, "A roadmap for implementing minichannels in refrigeration and air-conditioning systems - Current status and future directions," *Heat Transfer Engineering*, v 28, n 12, pp. 973-985, 2007.
- [32] B. London, M. Mahoney, W. Bingel, M. Calabrese, R.H. Bossi, D. Waldron, "Material Flow in Friction Stir Welding Monitored with Al-SiC and Al-W Composite Markers," *Friction stir welding and processing II*, TMS, Warrendale, PA, pp. 3–12, 2003.
- [33] P. A. Colegrove, H. R. Shercliff, 'Development of the Trivex™ Friction Stir Welding Tool Part I: 2 Dimensional Flow Modelling', *Science and Technology of Welding and Joining*, v 9, n 4, pp. 345-351, 2004.

- [34] P. A. Colegrove, H. R. Shercliff, 'Development of the Trivex™ Friction Stir Welding Tool Part II: 3 Dimensional Flow Modelling', *Science and Technology of Welding and Joining*, v 9, n 4, pp. 352-361, 2004.
- [35] O. Frigaard, Ø. Grong, O. T. Midling, "Modeling of heat flow phenomena in friction stir welding of aluminum alloys," *Inalco '98: Seventh International Conference on Joints in Aluminum*, Cambridge, UK, pp. 208-218, 1998.
- [36] M. Z. H. Khandkar, J. A. Khan, and A. P. Reynolds, "Prediction of temperature distribution and thermal history during friction stir welding: input torque based model," *Science and Technology of Welding and Joining*, v 8, pp. 165-174, 2003.
- [37] T. U. Seidel, A. P. Reynolds, "Two-dimensional friction stir welding process model based on fluid mechanics," *Science and Technology of Welding and Joining*, v 8, n 3, pp. 175-183, 2003.
- [38] H. Schmidt, J. Hattel and J. Wert, "An analytical model for the heat generation in friction stir welding," *Modeling and Simulation in Materials Science and Engineering*, v12, pp. 143-157, 2004.
- [39] P. Heurtier, M J. Jones, C. Desrayaud, J. H. Driver, F. Montheillet, D. Allehaux, "Mechanical and thermal modeling of Friction stir welding," *Journal of Materials Processing Technology*, v 171, pp. 348-357, 2006.
- [40] W. Arbegast, "Modeling friction stir joining as a metal working process," *Hot deformation of aluminum alloys III*, TMS, San Diego, CA, pp. 313-327, 2003.
- [41] G. G. Roy, R. Nandan, T. DebRoy, "Dimensionless correlation to estimate peak temperature during friction stir welding," *Science and Technology of Welding and Joining*, v11, n 5, pp. 606-608, 2006.
- [42] J.C. McClure, Z. Feng, W. Tang, X. Guo, "A Thermal Model Of Friction Stir Welding," *5th International Conference: Trends in Welding Research*, Pine Mountain, GA, USA, pp. 590-595, 1998.
- [43] D. Rosenthal, "The theory of moving sources of heat and its application to metal treatments," *Transactions of the ASME*, v 68, pp. 849-866, 1946.
- [44] P. Kalya, K. Krishnamurthy, R.S. Mishra, J.A. Baumann, "Specific Energy and Temperature Mechanistic Models for Friction Stir Processing of Al-F357,"

- Proceedings of Friction Stir Welding and Processing-IV, TMS, Orlando, FL, 2007.
- [45] T. Long, A. P. Reynolds, "Parametric studies of friction stir welding by commercial fluid dynamics simulation," *Science and Technology of Welding and Joining*, v 11, pp. 200–208, 2006.
- [46] J. H. Yan, M. A. Sutton, A. P. Reynolds, "Processing and banding in AA2524 and AA2024 friction stir welding," *Science and Technology of Welding and Joining*, v 12, pp. 390 – 401, 2007.
- [47] C. Blignault, D. G. Hattingh, G. H. Kruger, T. I. van Niekerk, M. N. James, "Friction Stir Weld Process Evaluation by Multi-Axial Transducer," *Measurement*, v 41, n 1 pp.32-43, 2008.
- [48] D. G. Hattingh, C. Blignault, T. I. van Niekerk, M. N. James, "Characterization of the Influences of FSW Tool Geometry on Welding Forces and Weld Tensile Strength Using an Instrumented Tool," accepted by the *Journal of Materials Processing Technology*, v 203, n 1-3, pp. 46-57, 2008.
- [49] W. Arbegast, "Friction Stir Welding and Processing," ASM International, 1st edition, Ed. R.S. Mishra, M. W. Mahoney, Chapter 13, pp 273-308, 2007.
- [50] D. G. Hattingh, T. I. van Niekerk, C. Blignault, G. Kruger, M. N. James, "Analysis of the FSW force footprint and its relationship with process parameters to optimise weld performance and tool design", Invited Paper (INVITED-2004-01), *IIW Journal Welding in the World*, v 48, n1-2, pp.50-58, 2004.

VITA

Nagarajan Balasubramanian was born and brought up in the city of Chennai (formerly Madras) in Tamil Nadu, India on the 13th of January 1981. He received his Bachelor of Engineering degree in Mechanical Engineering, First Class with Distinction, from the University of Madras's Faculty of Engineering in May 2002. He pursued his graduate studies from the University of Nevada, Las Vegas and achieved his Master of Science in Mechanical Engineering in December 2004. He obtained his Doctor of Philosophy degree in Mechanical Engineering from Missouri University of Science and Technology in August 2008.